Published for SISSA by Springer
Received: August 24, 2021
Revised: November 25, 2021
Accepted: December 26, 2021
Published: January 21, 2022

Dark matter in three-Higgs-doublet models with S_3 symmetry

W. Khater,[a] **A. Kunčinas,**[b] **O.M. Ogreid,**[c] **P. Osland**[d] **and M.N. Rebelo**[b]

[a] *Department of Physics, Birzeit University, P.O. Box 14, Birzeit, West Bank, Palestine*
[b] *Centro de Física Teórica de Partículas, CFTP, Departamento de Física, Instituto Superior Técnico, Universidade de Lisboa, Avenida Rovisco Pais nr. 1, 1049-001 Lisboa, Portugal*
[c] *Western Norway University of Applied Sciences, Postboks 7030, N-5020 Bergen, Norway*
[d] *Department of Physics and Technology, University of Bergen, Postboks 7803, N-5020 Bergen, Norway*

E-mail: Wkhater@birzeit.edu, Anton.Kuncinas@tecnico.ulisboa.pt, omo@hvl.no, Per.Osland@uib.no, rebelo@tecnico.ulisboa.pt

Abstract: Models with two or more scalar doublets with discrete or global symmetries can have vacua with vanishing vacuum expectation values in the bases where symmetries are imposed. If a suitable symmetry stabilises such vacua, these models may lead to interesting dark matter candidates, provided that the symmetry prevents couplings among the dark matter candidates and the fermions. We analyse three-Higgs-doublet models with an underlying S_3 symmetry. These models have many distinct vacua with one or two vanishing vacuum expectation values which can be stabilised by a remnant of the S_3 symmetry which survived spontaneous symmetry breaking. We discuss all possible vacua in the context of S_3-symmetric three-Higgs-doublet models, allowing also for softly broken S_3, and explore one of the vacuum configurations in detail. In the case we explore, only one of the three Higgs doublets is inert. The other two are active, and therefore the active sector, in many aspects, behaves like a two-Higgs-doublet model. The way the fermions couple to the scalar sector is constrained by the S_3 symmetry and is such that the flavour structure of the model is solely governed by the $V_{\rm CKM}$ matrix which, in our framework, is not constrained by the S_3 symmetry. This is a key requirement for models with minimal flavour violation. In our model there is no CP violation in the scalar sector. We study this model in detail giving the masses and couplings and identifying the range of parameters that are compatible with theoretical and experimental constraints, both from accelerator physics and from astrophysics.

Keywords: Beyond Standard Model, Higgs Physics

ArXiv ePrint: 2108.07026

https://doi.org/10.1007/JHEP01(2022)120

Contents

JHEP01(2022)120

1 Introduction

Cosmological observations, based on the standard cosmological model, $\Lambda_{\rm CDM}$, where CDM stands for cold dark matter, indicate that around a quarter of the total mass-energy density of the Universe is made up of Dark Matter (DM) [1].

In this paper a DM model based on the S_3-symmetric three-Higgs doublet model (3HDM) potential is studied in detail. In our framework the stability of the DM sector results from a $\mathbb{Z}_2$ symmetry which survives the spontaneous symmetry breakdown of the initial S_3 symmetry. One of the doublets provides the DM sector, while the other two are active. Therefore the active sector behaves in many ways like a two-Higgs doublet model (2HDM) [2, 3].

The paper is organised as follows. In section 2 a brief overview of the simplest implementations of scalar DM is presented, together with a list of references. First, we mention the Inert Doublet Model (IDM) [4, 5], a 2HDM which constitutes one of the first attempts at accounting for DM through the Higgs portal. Next we comment on implementations within 3HDMs. In section 3 we introduce the S_3-symmetric potential, and discuss the different vacua [6] starting from a real scalar potential. It has been shown that the S_3-symmetric potential allows for spontaneous CP violation [6, 7]. In this section we give the motivation to study a particular vacuum, denoted R-II-1a, on which the rest of our paper is based. With this choice of vacuum there is no CP violation in the scalar sector. Next, in section 4, we give the spectrum of masses of both the inert and the active sector of this model, specifying the rotations leading to the physical scalars, together with the scalar gauge couplings and the Yukawa couplings. The scalar-scalar couplings are listed in appendix A.

The theoretical and experimental constraints are imposed on the model in section 5. This is done step-by-step by imposing in succession a series of cuts and by performing the corresponding numerical analysis. We start with Cut 1: perturbativity, stability, unitarity checks, LEP constraints together with the value of the recently measured Higgs boson mass [8, 9] by plotting the allowed regions for masses and several of the parameters of the model. Next, we apply Cut 2: SM-like (Standard Model) gauge and Yukawa sector, electroweak precision observables and B physics; which further restrict the model as illustrated in that section. Finally, Cut 3 takes into account the limits imposed on the SM-like Higgs boson, h, by the decays $h \to \{\text{invisible},\ \gamma\gamma\}$, the DM relic density, and direct searches.

The micrOMEGAs code [10–12] is used at this stage to evaluate the cold dark matter relic density along with the decay widths and other astrophysical observables. The full impact of Cut 3 is discussed in section 6, where we also present a set of benchmarks for this model. Two different scenarios emerge right from the beginning of the numerical analysis presented in section 5, based on the ordering of the masses of the two neutral inert scalars, η and χ, which have opposite CP parities. The origin of the masses of these two fields is also different in terms of parameters of the potential. Cut 3 removes the possibility of having the η scalar lighter than χ. As a result, in this model only χ can play the rôle of DM. We also conclude that there are no good DM candidates for high mass values as is explained in our discussion. In section 7 we present our conclusions. There are several appendices where features of the model and details of our analysis are given.

2 Scalar dark matter

One of the simplest extensions of the SM which could accommodate DM is obtained by adding a scalar singlet. With an explicit $\mathbb{Z}_2$ symmetry, to prevent specific decay channels, this extension could yield a viable DM candidate [13–18]. Direct detection constraints were studied [19–22] based on the LHC data. The parameter space of these models was further constrained after the Higgs boson discovery [23–29]. While being the subject of specific exclusion criteria, in general, two DM regions were identified: a low-mass region 55–63 GeV and a high-mass region above around 100-500 GeV, depending on the implementation. In alternative, the scalar singlet DM can be stabilised by a different symmetry, such as $\mathbb{Z}_3$, which was considered in refs. [30, 31].

A DM candidate can also be introduced through non-trivial $\mathrm{SU}(2)_L$ scalar n-tuples. In ref. [32] a class of so-called minimal dark matter (MDM) multiplets was proposed. The key aspect of these models is to extend the SM by additional scalar multiplets with minimal quantum numbers (spin, isospin, hypercharge) to accommodate the DM candidate. The MDM models were further on studied in refs. [33–40].

2.1 The Inert Doublet Model

One of the most popular models, capable of accommodating DM, is the IDM [4, 5]. The IDM accommodates DM in the form of a neutral scalar: the lightest neutral member of an inert SU(2) Higgs doublet added to the SM. In addition to providing an economical accommodation of DM, the IDM also offers a mechanism for generating neutrino masses [41–43]. The IDM was studied extensively some ten years ago [36, 44–58]. Assuming the Higgs mass to be around 120 GeV, two DM mass regions were identified: a low and intermediate-mass region, from about 5 GeV to around 100 GeV (allowing for a heavy Higgs up to 500 GeV, this DM mass region would extend up to 160 GeV), and a high-mass region, beyond about 535 GeV. Above some 80 GeV, the annihilation in the early Universe to two gauge bosons (W^+W^- or ZZ) becomes very fast and the relic DM density would be too low. In addition, annihilation into two SM-like Higgs bosons is possible and is controlled by the effective λ_L coupling (parameterising the Higgs-DM-DM coupling), for small λ_L values the

JHEP01(2022)120

overall effect is negligible. Eventually, for sufficiently heavy DM particles, above approximately 500–535 GeV, the annihilation rate drops and as a result the DM density is again compatible with the data.

When the mass splitting between the DM candidate and the other scalars in the inert sector is sufficiently small, coannihilation effects get stronger. As a result, if the Higgs-DM-DM coupling, λ_L, has a suitable value, a relic density in agreement with observation can be achieved. For a fixed mass splitting with an increasing DM mass the absolute value of the λ_L coupling should increase to satisfy the experimental relic density value. On the other hand, for a fixed λ_L value, if the mass splittings are increased, the relic density decreases. The relic density depends also on the sign of λ_L. Interplay of these parameters may result in an acceptable relic density for the DM candidate of several TeV.

With the Higgs boson discovery [8, 9], it was pointed out that the decay width of the Higgs boson to two photons and invisible particles could further constrain the IDM [59–62]. It was found [63, 64] that with both astroparticle and collider constraints taken into account the DM mass region below 45–50 GeV is ruled out, and thus a minimal mass threshold is set. Later, the whole low- and intermediate-mass region was shown to be consistent with observations for the DM candidate with masses 55–74 GeV [65]. Although the high-mass region, above 500 GeV, requires severe fine-tuning it is still compatible with data. The region with the DM masses 74–500 GeV is still possible: the exclusion of a given mass region in the parameter space depends on whether one requires the IDM to provide a single component DM candidate to generate all relic density or just partially contribute to the DM relic density. More recently, ref. [66] confirmed earlier mass-range observations of the IDM and provided a set of benchmarks for e^+e^- studies, for IDM detection at potential e^+e^- colliders (ILC, CLIC) see refs. [67–69]. The aforementioned DM mass ranges are sketched in figure 1, together with those of some 3HDMs and that of the model (R-II-1a) explored here.

The main reasons some mass regions are *excluded*, are qualitatively as follows:

- Below $m_{\rm DM} = \mathcal{O}(50)$ GeV, it would annihilate too fast in the early Universe via off-shell Higgs bosons decaying to fermions. For $m_{\rm DM} \gtrsim 5$ GeV the leading contribution is from decay into b-quarks. Also, much of this range is excluded by LUX [75], by PandaX-II [76], and by XENON1T [77] data.

- In the case of small mass splitting, resonant coannihilation into gauge bosons occurs for 40–45 GeV. Another resonant coannihilation, mass splitting independent, at $m_{\rm DM} \sim 60$ GeV is due to annihilation into the Higgs boson, dependent on λ_L.

- In the region between $\mathcal{O}(80)$ GeV and $\mathcal{O}(m_h)$ it annihilates too fast via a pair of gauge or Higgs bosons. The latter channel, however, depends on λ_L.

- In the region from $\mathcal{O}(m_h)$ to $\mathcal{O}(500)$ GeV it annihilates too fast via two on- or off-shell gauge bosons. Depending on the λ_L value, annihilation into a pair of Higgs bosons can become significant. Also, in this region, annihilation into t-quarks becomes available.

JHEP01(2022)120

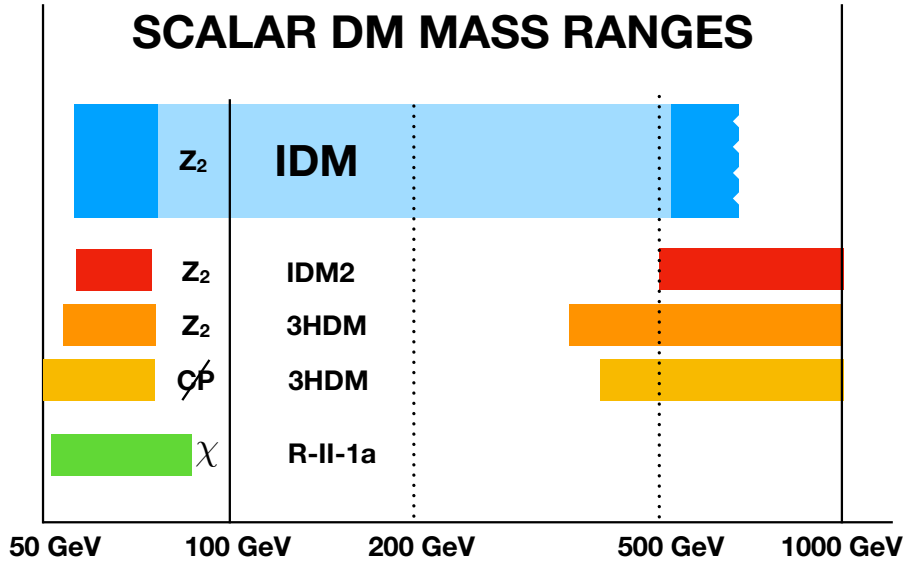

Figure 1. Sketch of allowed DM mass ranges up to 1 TeV in various models. Blue: IDM according to refs. [65, 66], the pale region indicates a non-saturated relic density. Red: IDM2 [70]. Ochre: 3HDM without [71–73] and with CP violation [74]. Green: the R-II-1a χ model presented in this paper.

- Above $\mathcal{O}(500)$ GeV an important mechanism is due to the coupling to longitudinal vector bosons [36]. With an increasing DM mass the relic density would grow. At some tens of TeV, interactions would become non-perturbative as a large value of λ_L would be required to match the DM relic density value. Coannihilations between all scalars from the inert doublet become important in the limit of degeneracy.

The exact mass values where these phenomena set in, depend on details of the model and the adopted experimental constraints.

2.2 3HDMs

In models with three scalar doublets one has more flexibility in accommodating dark matter:

1. By having two non-inert doublets along with one inert doublet [70, 78–80].
2. By having one non-inert doublet along with two inert doublets.

This latter approach has been pursued by various groups [71–74, 81–85]. The models studied in refs. [81, 83] assume an S_3-symmetric 3HDM potential, and take the S_3 singlet to represent the SM-like active doublet. There are then two inert doublets with zero vacuum expectation value (vev), corresponding to R-I-1 in our terminology in table 1 below. This model has three mass degeneracies: in the charged sector as well as in the CP-odd and CP-even neutral sectors of the S_3 doublet, as discussed in detail in ref. [86]. In all these models, like in the original IDM, the lightest neutral scalar in the inert sector is prevented from decaying to SM particles by a $\mathbb{Z}_2$ symmetry. In refs. [81, 83] the $\mathbb{Z}_2$ symmetry is softly broken, in order to lift the degeneracy, leading to consistent models with mass, at least, in the range 40–150 GeV [83].

JHEP01(2022)120

In refs. [71–73], a $\mathbb{Z}_2$-symmetric potential is constructed, and again the vacuum with two vanishing vevs is studied, yielding a model with two inert doublets. The authors point out that having more inert fields allows for more coannihilation channels, and opens up the parameter space compared to the IDM. Consistent models are found with mass in the range 53 to 77 GeV. Also, it was found that the high-mass region, which for the IDM requires a mass above some 500–525 GeV, can give consistent models with mass down to 360 GeV [72].

In ref. [74], the $\mathbb{Z}_2$-symmetric 3HDM is studied, with two inert doublets and a new ingredient being explicit CP violation via complex coefficients in the $\mathbb{Z}_2$-symmetric potential. This allows for more parameters, but only a modest extension of the mass ranges allowed by the CP-conserving 3HDM discussed above is found.

Finally, one can stabilise DM by a $\mathbb{Z}_3$ symmetry, rather than the $\mathbb{Z}_2$ symmetry [84, 85]. In this case, two-component DM is considered.

3 The S_3-symmetric models

Our philosophy here is to first identify vacua with at least one vanishing vev as possible frameworks for a DM model. We shall work in the irreducible representation, where we have two SU(2) doublets, h_1 and h_2 in a doublet of S_3, and one S_3 singlet denoted h_S. The Higgs doublets with a vanishing vev are labelled as "inert", since their lightest member (assumed neutral) could be DM. They are listed in table 1 below. Some of these are stabilised by a surviving symmetry of the potential, whereas others would require an imposed $\mathbb{Z}_2$ symmetry. The general S_3-symmetric scalar potential is invariant under $\mathbb{Z}_2 : h_1 \to -h_1$. We do not consider other mechanisms which would stabilise the DM candidate.

Some of these vacua are associated with massless states, hence we shall allow for soft breaking of the S_3 symmetry in the potential [86], noting that soft breaking is not possible in the Yukawa sector. When introducing soft breaking terms, the constraints will change. However, we will retain the nomenclature of the unbroken case from which they originate, thus when adding soft-breaking terms to R-I-1, we denote it r-I-1.

3.1 The scalar potential

In terms of the S_3 singlet ($\mathbf{1} : h_S$) and doublet ($\mathbf{2} : (h_1\, h_2)^{\mathrm{T}}$) fields, the S_3-symmetric potential can be written as [87–89]:

$$V_2 = \mu_0^2 h_S^\dagger h_S + \mu_1^2 (h_1^\dagger h_1 + h_2^\dagger h_2), \tag{3.1a}$$

$$\begin{aligned} V_4 = {} & \lambda_1 (h_1^\dagger h_1 + h_2^\dagger h_2)^2 + \lambda_2 (h_1^\dagger h_2 - h_2^\dagger h_1)^2 + \lambda_3 [(h_1^\dagger h_1 - h_2^\dagger h_2)^2 + (h_1^\dagger h_2 + h_2^\dagger h_1)^2] \\ & + \lambda_4 [(h_S^\dagger h_1)(h_1^\dagger h_2 + h_2^\dagger h_1) + (h_S^\dagger h_2)(h_1^\dagger h_1 - h_2^\dagger h_2) + \text{h.c.}] + \lambda_5 (h_S^\dagger h_S)(h_1^\dagger h_1 + h_2^\dagger h_2) \\ & + \lambda_6 [(h_S^\dagger h_1)(h_1^\dagger h_S) + (h_S^\dagger h_2)(h_2^\dagger h_S)] + \lambda_7 [(h_S^\dagger h_1)(h_S^\dagger h_1) + (h_S^\dagger h_2)(h_S^\dagger h_2) + \text{h.c.}] \\ & + \lambda_8 (h_S^\dagger h_S)^2. \end{aligned} \tag{3.1b}$$

Note that there are two coefficients in the potential that could be complex, thus CP can be broken explicitly. For simplicity, we have chosen all coefficients to be real. In spite of this choice there remains the possibility of breaking CP spontaneously.

JHEP01(2022)120

In the irreducible representation, the S_3 doublet and singlet fields will be decomposed as

$$h_i = \begin{pmatrix} h_i^+ \\ (w_i + \eta_i + i\chi_i)/\sqrt{2} \end{pmatrix}, \quad i = 1, 2, \qquad h_S = \begin{pmatrix} h_S^+ \\ (w_S + \eta_S + i\chi_S)/\sqrt{2} \end{pmatrix}, \tag{3.2}$$

where the w_i and w_S parameters can be complex.

The symmetry of the potential can be softly broken by the following terms [86]:

$$\begin{aligned} V_2' = \mu_2^2 \left(h_1^\dagger h_1 - h_2^\dagger h_2\right) + \frac{1}{2}\nu_{12}^2 \left(h_1^\dagger h_2 + \text{h.c.}\right) \\ + \frac{1}{2}\nu_{01}^2 \left(h_S^\dagger h_1 + \text{h.c.}\right) + \frac{1}{2}\nu_{02}^2 \left(h_S^\dagger h_2 + \text{h.c.}\right). \end{aligned} \tag{3.3}$$

In accordance with the previous simplification of couplings we assume that the soft terms are real. Soft symmetry-breaking terms are required whenever we work with solutions with $\lambda_4 = 0$ since in this case most vacua lead to massless scalar states, Goldstone bosons of an O(2) symmetry resulting from this choice. In our analysis we shall not make use of these terms.

We recall that in order for a doublet to accommodate a DM candidate it must have a vanishing vev, since otherwise it would decay via its gauge couplings, e.g., the SW^+W^- and SZZ couplings.

3.2 The Yukawa interaction

Whenever the singlet vev, w_S, is different from zero we can construct a trivial Yukawa sector, $\mathcal{L}_Y \sim 1_f \otimes 1_h$. In this case, the fermion mass matrices are:

$$\mathcal{M}_u = \frac{1}{\sqrt{2}} \text{diag}\left(y_1^u,\, y_2^u,\, y_3^u\right) w_S^*, \tag{3.4a}$$

$$\mathcal{M}_d = \frac{1}{\sqrt{2}} \text{diag}\left(y_1^d,\, y_2^d,\, y_3^d\right) w_S, \tag{3.4b}$$

where y's are the Yukawa couplings of appropriate fermions.

Another possibility is when fermions transform non-trivially under S_3, with a Yukawa Lagrangian written schematically as $\mathcal{L}_Y \sim (2 \oplus 1)_f \otimes (2 \oplus 1)_h$, one doublet and one singlet of S_3,

$$\mathbf{2} : (Q_1\, Q_2)^{\mathrm{T}},\ (u_{1R}\, u_{2R})^{\mathrm{T}},\ (d_{1R}\, d_{2R})^{\mathrm{T}} \quad \text{and} \quad \mathbf{1} : Q_3,\ u_{3R},\ d_{3R}.$$

Such structure yields the mass matrix for each quark sector (d and u) of the form

$$\mathcal{M}_u = \frac{1}{\sqrt{2}} \begin{pmatrix} y_1^u w_S^* + y_2^u w_2^* & y_2^u w_1^* & y_4^u w_1^* \\ y_2^u w_1^* & y_1^u w_S^* - y_2^u w_2^* & y_4^u w_2^* \\ y_5^u w_1^* & y_5^u w_2^* & y_3^u w_S^* \end{pmatrix}, \tag{3.5a}$$

$$\mathcal{M}_d = \frac{1}{\sqrt{2}} \begin{pmatrix} y_1^d w_S + y_2^d w_2 & y_2^d w_1 & y_4^d w_1 \\ y_2^d w_1 & y_1^d w_S - y_2^d w_2 & y_4^d w_2 \\ y_5^d w_1 & y_5^d w_2 & y_3^d w_S \end{pmatrix}. \tag{3.5b}$$

JHEP01(2022)120

If, for simplicity we assume all y's to be real, then a complex Cabibbo-Kobayashi-Maskawa (CKM) matrix would have to be generated from complex vacua. As we point out in the sequel, in some cases realistic quark masses and mixing can only be generated if the quarks are taken to be S_3 singlets and only couple to h_S, which requires complex Yukawa couplings as in the SM. On the other hand, even in some of the cases when the vevs are complex, the CKM matrix is not always complex.

The hermitian quantity,

$$\mathcal{H}_f = \mathcal{M}_f \mathcal{M}_f^\dagger, \tag{3.6}$$

is going to be useful in our discussion. The fermion mass matrices $\mathcal{M}_f$ are diagonalised in terms of the left-handed and the right-handed fermion rotation matrices, which, in general, are not equal. However, the quantity $\mathcal{M}_f \mathcal{M}_f^\dagger$ is diagonalised in terms of the left-handed rotation matrix only, and $\mathcal{M}_f^\dagger \mathcal{M}_f$ accordingly in terms of the right-handed rotation matrix. The eigenvalues of $\mathcal{H}_f$ will be the squared fermion masses.

It is instructive to count the number of parameters available in these models, and compare with the number of physical quantities to be fitted. The full Yukawa sector, eq. (3.5), has 10 parameters (5 y_i^d and 5 y_i^u). If $w_S = 0$, this number is reduced to 6 ($y_1^{(u,d)} = y_3^{(u,d)} = 0$). If either $w_1 = 0$ or $w_2 = 0$, we still have 10 parameters, but if both are zero, $w_1 = w_2 = 0$, the number is reduced to 4. The available parameters will be "used" to fit 6 quark masses plus 4 parameters of the CKM matrix. Apart from that, the most general vacuum configuration is given by 3 absolute values and 2 complex phases.

As we are interested in a DM candidate, one of the requirements is to have a field with a vanishing vacuum expectation value. Let us briefly consider what happens with the Yukawa sector in this case. When the DM candidate resides in the scalar S_3 singlet, $w_S = 0$, we need the fermions to couple to the S_3 doublet, schematically represented by $\mathcal{L}_Y \sim 2_f \otimes 2_h$. In some cases, the DM candidate can reside in the scalar S_3 doublet. To keep the notation simple, we still write the Yukawa sector as $\mathcal{L}_Y \sim (2 \oplus 1)_f \otimes (2 \oplus 1)_h$, as the general form of the fermion mass matrices persists. However, in order to stabilise the DM candidate one needs to introduce an additional $\mathbb{Z}_2$ symmetry in the Yukawa sector to decouple a specific inert doublet from the fermionic sector.

3.3 Vacua with at least one vanishing vev

In table 1, we list the vacua of the S_3-symmetric potential that could accommodate DM [6]. The vacua will be represented in the form

$$(w_1, w_2, w_S)\,. \tag{3.7}$$

Whenever $\langle h_S^0 \rangle \neq 0$ we indicate that the fermions may transform trivially under S_3. This is the simplest choice. In all other cases we need them to transform non-trivially in order to acquire masses. Whenever $\lambda_4 = 0$, the scalar potential acquires an additional O(2) symmetry between h_1 and h_2, which could be spontaneously broken. This breaking leads to one massless neutral scalar, see ref. [86] for a classification of massless states. Another interesting feature is that the scalar potential with the $\lambda_4 = 0$ constraint will have two additional $\mathbb{Z}_2$ symmetries beyond $h_1 \to -h_1$, involving h_2 and h_S. The symmetry $h_1 \to -h_1$

JHEP01(2022)120

Vacuum	vevs	λ_4	symmetry	# massless states	fermions under S_3
R-I-1	$(0,0,w_S)$	$\surd$	S_3, $h_1 \to -h_1$	none	trivial
R-I-2a	$(w,0,0)$	$\surd$	S_2	none	non-trivial
R-I-2b,2c	$(w,\pm\sqrt{3}w,0)$	$\surd$	S_2	none	non-trivial
R-II-1a	$(0,w_2,w_S)$	$\surd$	S_2, $h_1 \to -h_1$	none	trivial
R-II-2	$(0,w,0)$	0	S_2, $h_1 \to -h_1, h_S \to -h_S$	1	non-trivial
R-II-3	$(w_1,w_2,0)$	0	$h_S \to -h_S$	1	non-trivial
R-III-s	$(w_1,0,w_S)$	0	$h_2 \to -h_2$	1	trivial
C-I-a	$(\hat{w}_1,\pm i\hat{w}_1,0)$	$\surd$	cyclic $\mathbb{Z}_3$	none	non-trivial
C-III-a	$(0,\hat{w}_2 e^{i\sigma_2},\hat{w}_S)$	$\surd$	S_2, $h_1 \to -h_1$	none	trivial
C-III-b	$(\pm i\hat{w}_1,0,\hat{w}_S)$	0	$h_2 \to -h_2$	1	trivial
C-III-c	$(\hat{w}_1 e^{i\sigma_1},\hat{w}_2 e^{i\sigma_2},0)$	0	$h_S \to -h_S$	2	non-trivial
C-IV-a	$(\hat{w}_1 e^{i\sigma_1},0,\hat{w}_S)$	0	$h_2 \to -h_2$	2	trivial

Table 1. S_3 vacua that might accommodate DM due to a vanishing vev [6]. The "hat", $\hat{w}_i$, denotes an absolute value. See the text for further explanations.

is a symmetry of the potential in the irreducible representation. If h_1 does not acquire a vev it remains as an unbroken symmetry. Column 2 lists the vevs in the irreducible representation. S_2 and S_3 symmetry in the fourth column refer to remnant symmetries explicit in the defining representation, as does "cyclic $\mathbb{Z}_3$". For $\lambda_4 \neq 0$ real vacua can at most break $S_3 \to S_2$ [90]. Whenever $\lambda_4 = 0$ the S_3 symmetry can be fully broken by real vacua.

Below, we indicate some pros and cons of different vacua of S_3-3HDM, following the nomenclature of ref. [6].

- **R-I-1: (0, 0, w_S).**
  This case might result in a viable DM candidate. A related case was studied in refs. [81, 83]. In order to stabilise h_2 they forced $\lambda_4 = 0$ and found that this model may result in a viable DM candidate.

  Scalar sector: the DM candidate resides in h_1 and thus is automatically stabilised. There are three pairs of mass-degenerate states: a charged pair and two neutral pairs. In principle, one could lift this degeneracy by softly breaking the S_3 symmetry of the scalar potential. The only possible soft breaking term is μ_2^2. If this term is present, there are no mass degeneracies. In addition, it is possible to stabilise the h_2 doublet by forcing $\lambda_4 = 0$. There is no spontaneous symmetry breaking associated with the inert doublets and therefore no Goldstone states would arise due to spontaneously broken O(2).

  Yukawa sector: $\mathcal{L}_Y \sim 1_f \otimes 1_h$ can give realistic fermion masses. Due to freedom of parameters, this can give a realistic CKM matrix and no flavour-changing neutral currents (FCNC).

JHEP01(2022)120

- **R-I-2a: $(w, 0, 0)$.**
  The Yukawa sector is unrealistic.

  Scalar sector: the $\mathbb{Z}_2$ symmetry is preserved for $(h_2, h_S) \to -(h_2, h_S)$, or equivalently this translates into $h_1 \to -h_1$, and thus we have two stabilised inert doublets.

  Yukawa sector: $\mathcal{L}_Y \sim 2_f \otimes 2_h$ results in $\det(\mathcal{H}_f) = 0$. This indicates that one of the fermion mass eigenvalues vanishes, i.e., there will be a massless fermion.

- **R-I-2b,2c: $(w, \pm\sqrt{3}w, 0)$.**
  The S_3 symmetry of the scalar potential needs to be softly broken. The Yukawa sector is unrealistic.

  Scalar sector: there is mixing present in the mass-squared matrix as $\lambda_4 \neq 0$ and thus DM is not stabilised. If we artificially put $\lambda_4 = 0$, one of the neutral states would become massless. The DM is left stabilised only if the soft breaking term μ_2^2 together with ν_{12}^2 are introduced.

  Yukawa sector: $\mathcal{L}_Y \sim 2_f \otimes 2_h$ results in $\det(\mathcal{H}_f) = 0$.

- **R-II-1a: $(0, w_2, w_S)$.**
  This case results in a viable DM candidate provided that the Yukawa sector is trivial.

  Scalar sector: the DM candidate resides in h_1 and thus is automatically stabilised.

  Yukawa sector: $\mathcal{L}_Y \sim (2 \oplus 1)_f \otimes (2 \oplus 1)_h$ can give realistic fermion masses. The CKM matrix splits into a block-diagonal form and thus is unrealistic. However, there is another possibility to construct the Yukawa Lagrangian of the form $\mathcal{L}_Y \sim 1_f \otimes 1_h$.

- **R-II-2: $(0, w, 0)$.**
  The S_3 symmetry of the scalar potential needs to be softly broken. The Yukawa sector is unrealistic.

  Scalar sector: due to $\lambda_4 = 0$, $\mathbb{Z}_2$ is preserved for both h_1 and h_S. The $\lambda_4 = 0$ constraint results in an additional Goldstone state. The only soft breaking term which does not survive minimisation is ν_{12}^2. Also, ν_{02}^2 cannot be the only soft breaking term as then the massless state would survive. Then, the μ_2^2 and ν_{01}^2 couplings are free parameter as those do not depend on the minimisation conditions. The coupling ν_{02}^2 would require $\lambda_4 \neq 0$ and therefore DM is only stabilised in h_1.

  Yukawa sector: $\mathcal{L}_Y \sim 2_f \otimes 2_h$ can give realistic masses. However, the CKM matrix is split into a block-diagonal form.

- **R-II-3: $(w_1, w_2, 0)$.**
  The S_3 symmetry of the scalar potential needs to be softly broken. The Yukawa sector is unrealistic.

  Scalar sector: due to $\lambda_4 = 0$, $\mathbb{Z}_2$ is preserved for h_S. An additional Goldstone boson is present. The possible softly broken couplings are μ_2^2 and ν_{12}^2. If μ_2^2 is the only term present, for consistency $\nu_{12}^2 = 0$, this would require to impose either $w_1 = 0$ or

JHEP01(2022)120

$w_2 = 0$. When ν_{12}^2 is considered, it results in $w_1 = w_2$. It is also possible to have both terms present simultaneously.

Yukawa sector: $\mathcal{L}_Y \sim 2_f \otimes 2_h$ can give realistic fermion mass eigenvalues. However, the CKM matrix is unrealistic and there are no free parameters to control FCNC. The Yukawa sector results in six degrees of freedom: three from the u-type couplings and three from the d-type couplings. In case of the model with both couplings, r-II-3-μ_2^2-ν_{12}^2, there is an additional degree of freedom in terms of the ratio between the vevs w_1 and w_2.

- **R-III-s: $(w_1, 0, w_S)$.**
  This case might result in a viable DM candidate provided that the S_3 symmetry of the scalar potential is softly broken.

  Scalar sector: due to $\lambda_4 = 0$, $\mathbb{Z}_2$ is preserved for h_2. An additional Goldstone boson is present. Possible soft symmetry breaking terms are μ_2^2 and ν_{01}^2. Both of these couplings are unconstrained by the potential. In ref. [6] this vacuum with w_1 complex was denoted as C-IV-a and it was pointed out that the constraints made it real, therefore there is no need for λ_7 to be zero.

  Yukawa sector: $\mathcal{L}_Y \sim (2 \oplus 1)_f \otimes (2 \oplus 1)_h$ can give realistic fermionic masses and the CKM matrix. However, there are FCNC present in this case. In total, there are ten Yukawa couplings and a ratio between vacuum values. Due to such high number of free parameters it might be possible to control the overall effect of FCNC. There is also a possibility to construct the Yukawa Lagrangian of the form $\mathcal{L}_Y \sim 1_f \otimes 1_h$.

- **C-I-a: $(\hat{w}_1, \pm i\hat{w}_1, 0)$.**
  Both the scalar and Yukawa sectors are unrealistic.

  Scalar sector: in order to stabilise DM in h_S, we are forced to impose $\lambda_4 = 0$. In general, this model results in two neutral mass-degenerate pairs. No soft symmetry breaking terms survive and thus there are no c-I-a models.

  Yukawa sector: $\mathcal{L}_Y \sim 2_f \otimes 2_h$ can give realistic fermion masses. However, the CKM matrix is split into a block-diagonal form.

- **C-III-a: $(0, \hat{w}_2 e^{i\sigma_2}, \hat{w}_S)$.**
  This case might result in a viable DM candidate provided that the Yukawa sector is trivial.

  Scalar sector: the DM candidate resides in h_1 and thus is automatically stabilised.

  Yukawa sector: $\mathcal{L}_Y \sim (2 \oplus 1)_f \otimes (2 \oplus 1)_h$ can give realistic fermion masses. However, the CKM matrix is split into a block-diagonal form. Another possibility is to construct the Yukawa Lagrangian of the form $\mathcal{L}_Y \sim 1_f \otimes 1_h$.

- **C-III-b: $(\pm i\hat{w}_1, 0, \hat{w}_S)$.**
  This case might result in a viable DM candidate provided that the S_3 symmetry of the potential is softly broken.

JHEP01(2022)120

Scalar sector: due to $\lambda_4 = 0$, DM is stabilised in h_2. An additional Goldstone boson is present. The only possible soft symmetry breaking term is μ_2^2.

Yukawa sector: $\mathcal{L}_Y \sim (2 \oplus 1)_f \otimes (2 \oplus 1)_h$ results in realistic fermion masses and CKM matrix. This model has eleven free parameters. FCNC are present. Another possibility is to construct the Yukawa Lagrangian of the form $\mathcal{L}_Y \sim 1_f \otimes 1_h$.

- **C-III-c: $(\hat{w}_1 e^{i\sigma_1}, \hat{w}_2 e^{i\sigma_2}, 0)$.**
  The S_3 symmetry of the scalar potential needs to be softly broken. The Yukawa sector is most likely unrealistic.

  Scalar sector: due to $\lambda_4 = 0$, DM is stabilised in h_S. There are two massless states present in this model. Possible soft symmetry breaking terms are μ_2^2 and ν_{12}^2. Based on the soft breaking terms, vevs are altered: c-III-c-μ_2^2 results in $(\pm i\hat{w}_1, \hat{w}_2, 0)$, and c-III-c-$\nu_{12}^2$ in $(\hat{w}e^{i\sigma/2}, \hat{w}e^{-i\sigma/2}, 0)$, whereas the presence of both terms results in $(\hat{w}_1 e^{i\sigma_1}, \hat{w}_2 e^{i\sigma_2}, 0)$. For more details see [86].

  Yukawa sector: $\mathcal{L}_Y \sim 2_f \otimes 2_h$ can give realistic fermion mass eigenvalues. When the μ_2^2 or ν_{12}^2 terms are considered, there are seven free parameters. Preliminary check of the model with just ν_{12}^2 resulted in unrealistic CKM and a non-negligible FCNC contribution [91]. Most likely, exactly the same situation arises when μ_2^2 is added. However, the c-III-c-μ_2^2-ν_{12}^2 model has one additional free parameter due to unfixed vevs. Nevertheless, even if the CKM values can be fitted, there are still FCNCs that have to be controlled.

- **C-IV-a: $(\hat{w}_1 e^{i\sigma_1}, 0, \hat{w}_S)$.**
  This case might result in a viable DM candidate provided that the S_3 symmetry of the potential is softly broken.

  Scalar sector: due to $\lambda_4 = 0$, DM is stabilised in h_2. There are two massless states present in this model. Possible soft symmetry breaking terms are μ_2^2 and ν_{01}^2. In case of the c-IV-a-μ_2^2 model, the overall phase gets fixed $(i\hat{w}_1, 0, \hat{w}_S)$.

  Yukawa sector: $\mathcal{L}_Y \sim (2 \oplus 1)_f \otimes (2 \oplus 1)_h$ can give realistic fermion masses and CKM matrix. In total, there are twelve (eleven when only μ_2^2 is present) free parameters. The FCNCs are present. Another possibility is to construct the Yukawa Lagrangian of the form $\mathcal{L}_Y \sim 1_f \otimes 1_h$.

All in all, there are several models with a potential DM candidate. In our classification, which is summarised below, whenever unwanted Goldstone bosons are present, we refer to the need to include soft symmetry-breaking terms. Most of the models are ruled out due to unrealistic Yukawa sector. Full analysis of the Yukawa sector is out of scope of this paper. It should be noted that the non-trivial Yukawa sector might result in non-negligible FCNC and thus some of the models would be ruled out. Whenever the quarks transform trivially under S_3 they can only couple to one Higgs doublet, the S_3 singlet, and thus FCNC are not present. We have the following possible models, indicating where the DM candidate could reside and the Yukawa sector:

JHEP01(2022)120

- R-I-1/r-I-1-μ_2^2: DM $\sim h_1$ or DM $\sim (h_1,\, h_2)$, $\mathcal{L}_Y \sim 1_f \otimes 1_h$;
- R-II-1a: DM $\sim h_1$, $\mathcal{L}_Y \sim 1_f \otimes 1_h$;
- r-III-s-(μ_2^2, ν_{01}^2): DM $\sim h_2$, $\mathcal{L}_Y \sim (2 \oplus 1)_f \otimes (2 \oplus 1)_h$ or $\mathcal{L}_Y \sim 1_f \otimes 1_h$;
- C-III-a: DM $\sim h_1$, $\mathcal{L}_Y \sim 1_f \otimes 1_h$;
- c-III-b-μ_2^2: DM $\sim h_2$, $\mathcal{L}_Y \sim (2 \oplus 1)_f \otimes (2 \oplus 1)_h$ or $\mathcal{L}_Y \sim 1_f \otimes 1_h$;
- c-III-c-(μ_2^2, ν_{12}^2): DM $\sim h_S$, $\mathcal{L}_Y \sim 2_f \otimes 2_h$;
- c-IV-a-(μ_2^2, ν_{01}^2): DM $\sim h_2$, $\mathcal{L}_Y \sim (2 \oplus 1)_f \otimes (2 \oplus 1)_h$ or $\mathcal{L}_Y \sim 1_f \otimes 1_h$;

Despite the variety of models presented above, there are only three models with an S_3-symmetric scalar potential which is not softly broken and with a realistic Yukawa sector, that could result in a viable DM candidate. These models are R-I-1 $(0, 0, w_S)$, which was covered in refs. [81, 83] assuming a specific limit, R-II-1a $(0, w_2, w_S)$, and C-III-a $(0, \hat{w}_2 e^{i\sigma_2}, \hat{w}_S)$. Further on, we focus on the R-II-1a model and show that it could result in a viable DM candidate. The C-III-a model, which has spontaneous CP violation, will be presented elsewhere.

4 The R-II-1a model

4.1 Generalities

The R-II-1a vacuum is defined by [6]

$$\{0,\, w_2,\, w_S\}, \tag{4.1}$$

and the minimisation conditions are:

$$\mu_0^2 = \frac{1}{2}\lambda_4 \frac{w_2^3}{w_S} - \frac{1}{2}\lambda_a w_2^2 - \lambda_8 w_S^2, \tag{4.2a}$$

$$\mu_1^2 = -\left(\lambda_1 + \lambda_3\right) w_2^2 + \frac{3}{2}\lambda_4 w_2 w_S - \frac{1}{2}\lambda_a w_S^2, \tag{4.2b}$$

with

$$\lambda_a = \lambda_5 + \lambda_6 + 2\lambda_7. \tag{4.3}$$

The $\mathbb{Z}_2$ symmetry is preserved for:

$$h_1 \to -h_1, \quad \{h_2,\, h_S\} \to \pm\{h_2,\, h_S\}. \tag{4.4}$$

Hence, the inert doublet is associated with h_1, as $\langle h_1 \rangle = 0$.

A trivial Yukawa sector is assumed, $\mathcal{L}_Y \sim 1_f \otimes 1_h$, and thus the S_3 singlet is solely responsible for masses of fermions, making w_S a reference point. Therefore, we define the Higgs-basis rotation angle as:

$$\tan\beta = \frac{w_2}{w_S}. \tag{4.5}$$

JHEP01(2022)120

After a suitable rephasing of the scalar doublets we chose $w_S > 0$. With w_2 possibly negative, the Higgs basis rotation angle will be in the range $\beta \in [-\frac{\pi}{2}, \frac{\pi}{2}]$. Therefore, the vevs can be parameterised as:

$$w_2 = v \sin\beta, \quad w_S = v \cos\beta, \quad w_2^2 + w_S^2 = v^2. \tag{4.6}$$

The Higgs basis rotation is given by:

$$\begin{aligned} \mathcal{R}_\beta = \frac{1}{v} \begin{pmatrix} v & 0 & 0 \\ 0 & w_2 & w_S \\ 0 & -w_S & w_2 \end{pmatrix} &= \begin{pmatrix} 1 & 0 & 0 \\ 0 & \cos\left(\frac{\pi}{2} - \beta\right) & \sin\left(\frac{\pi}{2} - \beta\right) \\ 0 & -\sin\left(\frac{\pi}{2} - \beta\right) & \cos\left(\frac{\pi}{2} - \beta\right) \end{pmatrix}, \\ &= \begin{pmatrix} 1 & 0 & 0 \\ 0 & \sin\beta & \cos\beta \\ 0 & -\cos\beta & \sin\beta \end{pmatrix}, \end{aligned} \tag{4.7}$$

so that

$$\mathcal{R}_\beta \begin{pmatrix} 0 \\ w_2 \\ w_S \end{pmatrix} = \begin{pmatrix} 0 \\ v \\ 0 \end{pmatrix}. \tag{4.8}$$

4.2 R-II-1a masses

4.2.1 Charged mass-squared matrix

The charged mass-squared matrix in the $\{h_1^+, h_2^+, h_S^+\}$ basis is given by:

$$\mathcal{M}^2_{\text{Ch}} = \begin{pmatrix} (\mathcal{M}^2_{\text{Ch}})_{11} & 0 & 0 \\ 0 & (\mathcal{M}^2_{\text{Ch}})_{22} & (\mathcal{M}^2_{\text{Ch}})_{23} \\ 0 & (\mathcal{M}^2_{\text{Ch}})_{23} & (\mathcal{M}^2_{\text{Ch}})_{33} \end{pmatrix}, \tag{4.9}$$

where

$$\left(\mathcal{M}^2_{\text{Ch}}\right)_{11} = -2\lambda_3 w_2^2 + \frac{5}{2}\lambda_4 w_2 w_S - \frac{1}{2}(\lambda_6 + 2\lambda_7) w_S^2, \tag{4.10a}$$

$$\left(\mathcal{M}^2_{\text{Ch}}\right)_{22} = \frac{1}{2} w_S \left[\lambda_4 w_2 - (\lambda_6 + 2\lambda_7) w_S\right], \tag{4.10b}$$

$$\left(\mathcal{M}^2_{\text{Ch}}\right)_{23} = -\frac{1}{2} w_2 \left[\lambda_4 w_2 - (\lambda_6 + 2\lambda_7) w_S\right], \tag{4.10c}$$

$$\left(\mathcal{M}^2_{\text{Ch}}\right)_{33} = \frac{1}{2}\frac{w_2^2}{w_S} \left[\lambda_4 w_2 - (\lambda_6 + 2\lambda_7) w_S\right]. \tag{4.10d}$$

The charged mass-squared matrix is diagonalisable by the rotation (4.7). Therefore, the mass eigenstates can be expressed as:

$$h^+ = h_1^+, \tag{4.11a}$$

$$G^+ = \sin\beta\, h_2^+ + \cos\beta\, h_S^+, \tag{4.11b}$$

$$H^+ = -\cos\beta\, h_2^+ + \sin\beta\, h_S^+, \tag{4.11c}$$

JHEP01(2022)120

with masses:

$$m_{h^+}^2 = -2\lambda_3 w_2^2 + \frac{5}{2}\lambda_4 w_2 w_S - \frac{1}{2}(\lambda_6 + 2\lambda_7) w_S^2, \tag{4.12a}$$

$$m_{H^+}^2 = \frac{v^2}{2w_S}\left[\lambda_4 w_2 - (\lambda_6 + 2\lambda_7)\, w_S\right]. \tag{4.12b}$$

Positivity of the squared masses requires the following constraints to be satisfied:

$$\lambda_4 > (\lambda_6 + 2\lambda_7)\cot\beta, \tag{4.13a}$$

$$\lambda_4 > \frac{4}{5}\lambda_3 \tan\beta + \frac{1}{5}(\lambda_6 + 2\lambda_7)\cot\beta. \tag{4.13b}$$

4.2.2 Inert-sector neutral mass-squared matrix

The mass terms of the neutral components of the h_1 doublet are already diagonal. The masses of the two neutral states are given by:

$$m_\eta^2 = \frac{9}{2}\lambda_4 w_2 w_S, \tag{4.14a}$$

$$m_\chi^2 = -2(\lambda_2 + \lambda_3) w_2^2 + \frac{5}{2}\lambda_4 w_2 w_S - 2\lambda_7 w_S^2. \tag{4.14b}$$

Positivity of the masses squared requires the following constraints to be satisfied:

$$\lambda_4 > \frac{4}{5}(\lambda_2 + \lambda_3)\tan\beta + \frac{4}{5}\lambda_7 \cot\beta, \tag{4.15a}$$

$$\lambda_4 \sin\beta > 0. \tag{4.15b}$$

4.2.3 Non-inert-sector neutral mass-squared matrix

The neutral mass-squared matrix is block-diagonal in the basis $\{\eta_2, \eta_S, \chi_2, \chi_S\}$. Therefore the mass-squared matrix can be split into two blocks:

$$\mathcal{M}^2_{\text{Neutral}} = \text{diag}\left(\mathcal{M}^2_{\eta-2S}, \mathcal{M}^2_{\chi-2S}\right), \tag{4.16}$$

where "2S" refers to the mixing of h_2 and h_S. The mass-squared matrix of the CP-odd sector is:

$$\mathcal{M}^2_{\chi-2S} = \begin{pmatrix} \left(\mathcal{M}^2_{\chi-2S}\right)_{11} & \left(\mathcal{M}^2_{\chi-2S}\right)_{12} \\ \left(\mathcal{M}^2_{\chi-2S}\right)_{12} & \left(\mathcal{M}^2_{\chi-2S}\right)_{22} \end{pmatrix}, \tag{4.17}$$

where

$$\left(\mathcal{M}^2_{\chi-2S}\right)_{11} = \frac{1}{2} w_S \left(\lambda_4 w_2 - 4\lambda_7 w_S\right), \tag{4.18a}$$

$$\left(\mathcal{M}^2_{\chi-2S}\right)_{12} = -\frac{1}{2} w_2 \left(\lambda_4 w_2 - 4\lambda_7 w_S\right), \tag{4.18b}$$

$$\left(\mathcal{M}^2_{\chi-2S}\right)_{22} = \frac{w_2^2}{2w_S}\left(\lambda_4 w_2 - 4\lambda_7 w_S\right). \tag{4.18c}$$

It can be diagonalised by performing the $\mathcal{R}_\beta$ rotation (4.7). The two CP-odd states are:

$$G^0 = \sin\beta\, \chi_2 + \cos\beta\, \chi_S, \tag{4.19a}$$

$$A = -\cos\beta\, \chi_2 + \sin\beta\, \chi_S, \tag{4.19b}$$

JHEP01(2022)120

with

$$m_A^2 = \frac{v^2}{2w_S}\left(\lambda_4 w_2 - 4\lambda_7 w_S\right). \tag{4.20}$$

Positivity of the squared masses requires

$$\lambda_4 > 4\lambda_7 \cot\beta. \tag{4.21}$$

The CP-even mass-squared matrix is:

$$\mathcal{M}^2_{\eta-2S} = \begin{pmatrix} \left(\mathcal{M}^2_{\eta-2S}\right)_{11} & \left(\mathcal{M}^2_{\eta-2S}\right)_{12} \\ \left(\mathcal{M}^2_{\eta-2S}\right)_{12} & \left(\mathcal{M}^2_{\eta-2S}\right)_{22} \end{pmatrix}, \tag{4.22}$$

where

$$\left(\mathcal{M}^2_{\eta-2S}\right)_{11} = \frac{1}{2} w_2 \left[4\left(\lambda_1+\lambda_3\right) w_2 - 3\lambda_4 w_S\right], \tag{4.23a}$$

$$\left(\mathcal{M}^2_{\eta-2S}\right)_{12} = -\frac{1}{2} w_2 \left[3\lambda_4 w_2 - 2\lambda_a w_S\right], \tag{4.23b}$$

$$\left(\mathcal{M}^2_{\eta-2S}\right)_{22} = \frac{1}{2w_S}\left(\lambda_4 w_2^3 + 4\lambda_8 w_S^3\right). \tag{4.23c}$$

The mass-squared matrix is diagonalisable by

$$\mathcal{R}_\alpha = \begin{pmatrix} \cos\alpha & \sin\alpha \\ -\sin\alpha & \cos\alpha \end{pmatrix}, \tag{4.24}$$

with

$$\tan(2\alpha) = \frac{2w_2 w_S(-3\lambda_4 w_2 + 2\lambda_a w_S)}{4(\lambda_1+\lambda_3)w_2^2 w_S - \lambda_4\left(w_2^3 + 3w_2 w_S^2\right) - 4\lambda_8 w_S^3}. \tag{4.25}$$

The CP-even states are:

$$h = \cos\alpha\,\eta_2 + \sin\alpha\,\eta_S, \tag{4.26a}$$

$$H = -\sin\alpha\,\eta_2 + \cos\alpha\,\eta_S, \tag{4.26b}$$

with masses:

$$m_h^2 = \frac{1}{4w_S^2}\left[4\left(\lambda_1+\lambda_3\right) w_2^2 w_S^2 + \lambda_4 w_2 w_S\left(w_2^2 - 3w_S^2\right) + 4\lambda_8 w_S^4 - w_S\Delta\right], \tag{4.27a}$$

$$m_H^2 = \frac{1}{4w_S^2}\left[4\left(\lambda_1+\lambda_3\right) w_2^2 w_S^2 + \lambda_4 w_2 w_S\left(w_2^2 - 3w_S^2\right) + 4\lambda_8 w_S^4 + w_S\Delta\right], \tag{4.27b}$$

where

$$\begin{aligned}\Delta^2 = {} & 16\left(\lambda_1+\lambda_3\right)^2 w_2^4 w_S^2 - 8\left(\lambda_1+\lambda_3\right) w_2^2 w_S\left[\lambda_4\left(w_2^3 + 3w_2 w_S^2\right) + 4\lambda_8 w_S^3\right] \\ & + 16\lambda_a^2 w_2^2 w_S^4 - 48\lambda_4\lambda_a w_2^3 w_S^3 + \lambda_4^2\left(w_2^6 + 42 w_2^4 w_S^2 + 9 w_2^2 w_S^4\right) \\ & + 8\lambda_4\lambda_8 w_2 w_S^3\left(w_2^2 + 3w_S^2\right) + 16\lambda_8^2 w_S^6.\end{aligned} \tag{4.28}$$

We identify the lighter state, h, as the SM-like Higgs boson.

JHEP01(2022)120

It should be noted that we identified the mass eigenstates of the CP-even sector without performing a rotation to the Higgs basis. Had we done that according to

$$\begin{pmatrix} h_1^{\mathrm{HB}} \\ h_2^{\mathrm{HB}} \\ h_S^{\mathrm{HB}} \end{pmatrix} \equiv \mathcal{R}_\beta \begin{pmatrix} h_1 \\ h_2 \\ h_S \end{pmatrix}, \tag{4.29}$$

the CP-even sector would have been diagonalised by the additional rotation

$$\mathcal{R}_{\alpha'} = \begin{pmatrix} \cos\alpha' & \sin\alpha' \\ -\sin\alpha' & \cos\alpha' \end{pmatrix}, \tag{4.30}$$

with

$$\alpha' = \alpha + \beta - \frac{\pi}{2}. \tag{4.31}$$

4.2.4 Mass eigenstates

In terms of the mass eigenstates, the SU(2) doublets can be written as:

$$h_1 = \begin{pmatrix} h^+ \\ \frac{1}{\sqrt{2}}(\eta + i\chi) \end{pmatrix}, \tag{4.32a}$$

$$h_2 = \begin{pmatrix} \sin\beta\, G^+ - \cos\beta\, H^+ \\ \frac{1}{\sqrt{2}}\left(\sin\beta\, v + \cos\alpha\, h - \sin\alpha\, H + i\left(\sin\beta\, G^0 - \cos\beta\, A\right)\right) \end{pmatrix}, \tag{4.32b}$$

$$h_S = \begin{pmatrix} \cos\beta\, G^+ + \sin\beta\, H^+ \\ \frac{1}{\sqrt{2}}\left(\cos\beta\, v + \sin\alpha\, h + \cos\alpha\, H + i\left(\cos\beta\, G^0 + \sin\beta\, A\right)\right) \end{pmatrix}, \tag{4.32c}$$

whereas in the Higgs basis the SU(2) doublets can be written as:

$$h_1^{\mathrm{HB}} = \begin{pmatrix} h^+ \\ \frac{1}{\sqrt{2}}(\eta + i\chi) \end{pmatrix}, \tag{4.33a}$$

$$h_2^{\mathrm{HB}} = \begin{pmatrix} G^+ \\ \frac{1}{\sqrt{2}}\left(v + \sin(\alpha+\beta)\, h + \cos(\alpha+\beta)\, H + iG^0\right) \end{pmatrix}, \tag{4.33b}$$

$$h_3^{\mathrm{HB}} = \begin{pmatrix} H^+ \\ \frac{1}{\sqrt{2}}\left(-\cos(\alpha+\beta)\, h + \sin(\alpha+\beta)\, H + iA\right) \end{pmatrix}. \tag{4.33c}$$

JHEP01(2022)120

The expressions for the squared masses can be inverted to yield the scalar potential couplings:

$$\lambda_1 = \frac{v^2\left[9\left(m_{h^+}^2 + \cos^2\alpha\, m_h^2 + \sin^2\alpha\, m_H^2\right) - m_\eta^2\right] - 9m_{H^+}^2 w_S^2}{18v^2w_2^2}, \tag{4.34a}$$

$$\lambda_2 = \frac{\left(m_{h^+}^2 - m_\chi^2\right)v^2 + \left(m_A^2 - m_{H^+}^2\right)w_S^2}{2v^2w_2^2}, \tag{4.34b}$$

$$\lambda_3 = \frac{\left(4m_\eta^2 - 9m_{h^+}^2\right)v^2 + 9m_{H^+}^2 w_S^2}{18v^2w_2^2}, \tag{4.34c}$$

$$\lambda_4 = \frac{2m_\eta^2}{9w_2w_S}, \tag{4.34d}$$

$$\lambda_5 = \frac{2m_{H^+}^2}{v^2} + \frac{w_2m_\eta^2 - \frac{9}{2}\sin(2\alpha)w_S(m_H^2 - m_h^2)}{9w_2w_S^2}, \tag{4.34e}$$

$$\lambda_6 = \frac{m_A^2 - 2m_{H^+}^2}{v^2} + \frac{m_\eta^2}{9w_S^2}, \tag{4.34f}$$

$$\lambda_7 = \frac{1}{18}\left(\frac{m_\eta^2}{w_S^2} - \frac{9m_A^2}{v^2}\right), \tag{4.34g}$$

$$\lambda_8 = \frac{9w_S^2\left(\sin^2\alpha\, m_h^2 + \cos^2\alpha\, m_H^2\right) - w_2^2m_\eta^2}{18w_S^4}. \tag{4.34h}$$

The model is invariant under a simultaneous transformation of

$$\begin{aligned} \beta &\to -\beta, & \alpha &\to \pi - \alpha, \\ \lambda_4 &\to -\lambda_4, & & \\ \{H^\pm,\, H,\, A\} &\to -\{H^\pm,\, H,\, A\}, & & \end{aligned} \tag{4.35}$$

which could have been adopted, but is not, in order to reduce ranges of parameters.

4.3 The R-II-1a couplings

Below, we quote the gauge and Yukawa couplings of the R-II-1a model. The scalar-sector couplings are collected in appendix A.

JHEP01(2022)120

4.3.1 Gauge couplings

After substituting the doublets in terms of the mass eigenstates (4.32) into the kinetic Lagrangian, the resulting terms are:

$$\mathcal{L}_{VVH} = \left[\frac{g}{2\cos\theta_W} m_Z Z_\mu Z^\mu + g m_W W^+_\mu W^{\mu-}\right][\sin(\alpha+\beta)h + \cos(\alpha+\beta)H], \tag{4.36a}$$

$$\begin{aligned}\mathcal{L}_{VHH} = &-\frac{g}{2\cos\theta_W} Z^\mu \left[\eta \overset{\leftrightarrow}{\partial_\mu} \chi - \cos(\alpha+\beta) h \overset{\leftrightarrow}{\partial_\mu} A + \sin(\alpha+\beta) H \overset{\leftrightarrow}{\partial_\mu} A\right] \\ &- \frac{g}{2}\Big\{ i W^+_\mu \Big[i h^- \overset{\leftrightarrow}{\partial^\mu} \chi + h^- \overset{\leftrightarrow}{\partial^\mu} \eta - \cos(\alpha+\beta) H^- \overset{\leftrightarrow}{\partial^\mu} h \\ &\qquad + \sin(\alpha+\beta) H^- \overset{\leftrightarrow}{\partial^\mu} H + i H^- \overset{\leftrightarrow}{\partial^\mu} A\Big] + \text{h.c.}\Big\} \\ &+ \left[ieA^\mu + \frac{ig}{2}\frac{\cos(2\theta_W)}{\cos\theta_W} Z^\mu\right]\left(h^+ \overset{\leftrightarrow}{\partial_\mu} h^- + H^+ \overset{\leftrightarrow}{\partial_\mu} H^-\right),\end{aligned} \tag{4.36b}$$

$$\begin{aligned}\mathcal{L}_{VVHH} = &\left[\frac{g^2}{8\cos^2\theta_W} Z_\mu Z^\mu + \frac{g^2}{4} W^+_\mu W^{\mu-}\right]\left(\eta^2 + \chi^2 + h^2 + H^2 + A^2\right) \\ &+ \Big\{\left[\frac{eg}{2} A^\mu W^+_\mu - \frac{g^2}{2}\frac{\sin^2\theta_W}{\cos\theta_W} Z^\mu W^+_\mu\right][\eta h^- + i\chi h^- - \cos(\alpha+\beta) h H^- \\ &\quad + \sin(\alpha+\beta) H H^- + i A H^-] + \text{h.c.}\Big\} \\ &+ \left[e^2 A_\mu A^\mu + eg\frac{\cos(2\theta_W)}{\cos\theta_W} A_\mu Z^\mu + \frac{g^2}{4}\frac{\cos^2(2\theta_W)}{\cos^2\theta_W} Z_\mu Z^\mu + \frac{g^2}{2} W^-_\mu W^{\mu+}\right] \\ &\times \left(h^- h^+ + H^- H^+\right),\end{aligned} \tag{4.36c}$$

where we have left out couplings involving Goldstone fields.

From the interaction terms ZZh and ZZH it follows that the states h and H are CP-even and therefore the state A is CP-odd. Provided that the h scalar is associated with the SM-like Higgs boson, from the interactions hZZ and $hW^\pm W^\mp$ it follows that the SM-like limit is reached for

$$\sin(\alpha+\beta) = 1. \tag{4.37}$$

4.3.2 Yukawa couplings

As noted earlier, there are two possibilities to construct the Yukawa Lagrangian:

$$\begin{aligned}&\mathcal{L}_Y \sim (2\oplus 1)_f \otimes (2\oplus 1)_h, \quad \text{and} \\ &\mathcal{L}_Y \sim 1_f \otimes 1_h.\end{aligned}$$

Although the first option can give realistic fermion masses, the CKM matrix splits into a block-diagonal form. We consider the trivial representation for fermions:[1]

$$-\mathcal{L}_Y = \overline{Q}^0_{iL} y^d_{ij} h_S d^0_{jR} + \overline{Q}^0_{iL} y^u_{ij} \tilde{h}_S u^0_{jR} + (\text{leptonic sector}) + \text{h.c.}, \tag{4.38}$$

[1] In our study neutrino masses are of no particular interest.

JHEP01(2022)120

where the Yukawa couplings $y_{ij}^{(u,d)}$ are assumed to be real, as mentioned earlier, and $\tilde{h}_S$ is the charge conjugated of h_S, i.e., $\tilde{h}_S = i\sigma_2 h_S^*$. The fermion mass matrices are to be transformed as the superscripts "0" on the fermion fields indicate a weak-basis field.

When considering the trivial Yukawa sector, the CKM matrix, $V_{\rm CKM} = V_u^\dagger V_d$, can be easily fixed to match the experimental value. Moreover, there is no naturally, at tree-level, occurring source responsible for FCNC. The scalar-fermion couplings can be extracted from eq. (4.38) by transforming into the fermion mass-eigenstates basis and multiplying the appropriate coefficients, next to the fields, by $-i$:

$$g\left(h\bar{f}f\right) = -i\frac{m_f}{v}\frac{\sin\alpha}{\cos\beta}, \qquad g\left(H\bar{f}f\right) = -i\frac{m_f}{v}\frac{\cos\alpha}{\cos\beta}, \tag{4.39a}$$

$$g\left(A\bar{u}u\right) = -\gamma_5\frac{m_u}{v}\tan\beta, \qquad g\left(A\bar{d}d\right) = \gamma_5\frac{m_d}{v}\tan\beta, \tag{4.39b}$$

and for the leptonic sector, the Dirac mass terms would lead to similar relations. The SM-like limit for the scalar h, $g_{h\bar{f}f}^{\rm SM} = -i\,m_f/v$, is restored at

$$\frac{\sin\alpha}{\cos\beta} = 1. \tag{4.40}$$

Finally, the charged scalar-fermion couplings are:

$$g\left(H^+\bar{u}_i d_j\right) = i\frac{\sqrt{2}}{v}\tan\beta\left[P_L m_u - P_R m_d\right]\left(V_{\rm CKM}\right)_{ij}, \tag{4.41a}$$

$$g\left(H^-\bar{d}_i u_j\right) = i\frac{\sqrt{2}}{v}\tan\beta\left[P_R m_u - P_L m_d\right]\left(V_{\rm CKM}^\dagger\right)_{ji}, \tag{4.41b}$$

$$g\left(H^+\bar{\nu}l\right) = -i\frac{\sqrt{2}m_l}{v}\tan\beta P_R, \tag{4.41c}$$

$$g\left(H^-\bar{l}\nu\right) = -i\frac{\sqrt{2}m_l}{v}\tan\beta P_L. \tag{4.41d}$$

The structure of the Yukawa couplings is the same as that of the 2HDM, Type I, except that our definition of $\tan\beta$ is the inverse, since the singlet vev is here taken as the reference (denominator):

$$(\tan\beta)_{\text{R-II-1a}} = \left(\frac{1}{\tan\beta}\right)_{\text{2HDM, Type I}}. \tag{4.42}$$

Note also that α is defined differently.

5 Model analysis

For simplicity, we introduce a generic notation for different scalars,

$$\varphi_i^\pm = \{h^\pm,\, H^\pm\},$$
$$\varphi_i = \{\eta,\, \chi\}.$$

Precise measurements of the $W^\pm$ and Z widths at LEP [92] forbid decays of the gauge bosons into a pair of scalars. In our case, the lower limits on the scalar masses are set by the

JHEP01(2022)120

following constraints: $m_{\varphi_i^\pm} > \frac{1}{2}m_Z$, and $m_{\varphi_i} + m_{h^\pm} > m_{W^\pm}$, and $m_\eta + m_\chi > m_Z$. Usually, a conservative lower bound for the charged masses $m_{\varphi_i^\pm} \geq 80$ GeV is adopted [93, 94]. We assume a slightly more generous lower bound of $m_{\varphi_i^\pm} \geq 70$ GeV.

The model is analysed using the following input:

- Mass of the SM-like Higgs is fixed at $m_h = 125.25\,\text{GeV}$ [95];
- The Higgs basis rotation angle $\beta \in [-\frac{\pi}{2},\ \frac{\pi}{2}]$ and the h-H diagonalisation angle $\alpha \in [0,\ \pi]$;
- The charged scalar masses $m_{\varphi_i^\pm} \in [0.07,\ 1]\,\text{TeV}$;
- The inert sector masses $m_{\varphi_i} \in [0,\ 1]\,\text{TeV}$. Either η or χ could be a DM candidate, whichever is lighter;
- The active sector masses $\{m_H,\ m_A\} \in [m_h,\ 1\ \text{TeV}]$;

For the numerical parameter scan, both theoretical and experimental constraints are evaluated. Based on the constraints, several cuts are defined and applied:

- Cut 1: perturbativity, stability, unitarity checks, LEP constraints;
- Cut 2: SM-like gauge and Yukawa sector, electroweak precision observables and B physics;
- Cut 3: $h \to \{\text{invisible},\ \gamma\gamma\}$ decays, DM relic density, direct searches;

with each of the subsequent constraint being superimposed over the previous ones.

5.1 Imposing theory constraints

Imposing the theory constraints discussed in appendix B, we can exclude parts of the parameter space, as illustrated in figure 2. Low values of w_2, and hence of β (see eq. (4.6)), are disfavoured by the R-II-1a model. This can be seen by inspecting the λ_1, λ_2, and λ_3 couplings (4.34), these couplings are proportional to $1/w_2^2$. A particularly instructive combination, expanded for small β, is

$$\lambda_1 + \lambda_3 \approx \frac{1}{6v^2\beta^2}\left(3m_h^2 + m_\eta^2\right), \tag{5.1}$$

with λ_1 minimised for $\alpha = \pi/2$. With a decreasing denominator $\sim \beta^2$, we want to control the overall value of $|\lambda_i|$, and therefore the value of the numerator must also decrease. The perturbativity constraint restricts large values of the λ_i couplings, see appendix B.3, and sets a limit $0 < \lambda_1 + \lambda_3 \leq 2\pi/3$ (A.4a). For $m_\eta^2 \ll 3m_h^2$, we arrive at the bound

$$\frac{3m_h^2}{4\pi v^2} \leq \sin^2\beta, \tag{5.2}$$

which means that $|\tan\beta| > 0.26$. For $m_\eta = m_h$ the bound is $|\tan\beta| > 0.30$.

JHEP01(2022)120

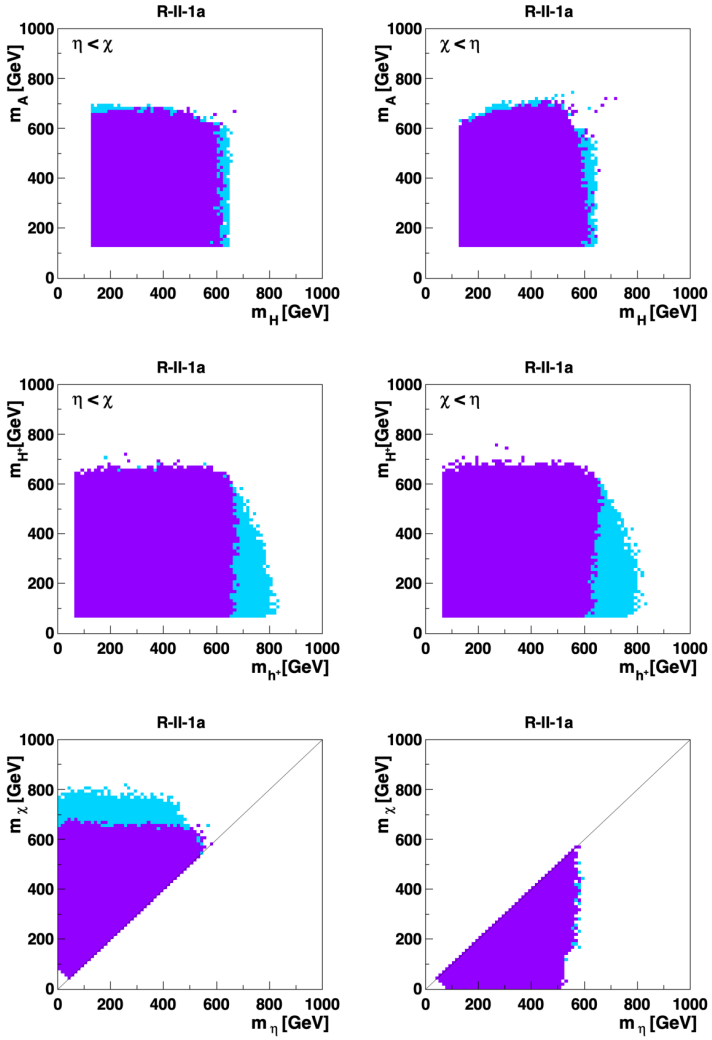

Figure 2. Scatter plots of masses that satisfy theory constraints, Cut 1, for both orderings of m_η and m_χ. Top: masses of the neutral states of the active doublets, H and A. Middle: masses of the charged states, $h^\pm$ and $H^\pm$. Bottom: masses of the neutral states of the inert doublet, η and χ. The light-blue region accommodates the 16π unitarity constraint, whereas the darker region satisfies the 8π constraint.

In our model fermions couple only to the h_S doublet. This can be used to put a limit on the $\tan\beta$ value. From the definition of the Yukawa couplings, $Y_f = \frac{\sqrt{2}m_f}{v\cos\beta}$, and the perturbativity requirement, $|Y_f| \leq 4\pi$, it follows that the most stringent bound comes from the heaviest state, which is $m_f = m_t$. For these values we find that $|\tan\beta| \leq 12.6$. While there would be Landau poles in the vicinity of this non-perturbative region, we note that other constraints prevent parameters from getting close.

Finally, we shall assume that the unitarity constraint is satisfied for the value of 16π rather than 8π, see appendix B.2. It turns out that points surviving all of the checks satisfy unitarity constraint at the value of 8π.

JHEP01(2022)120

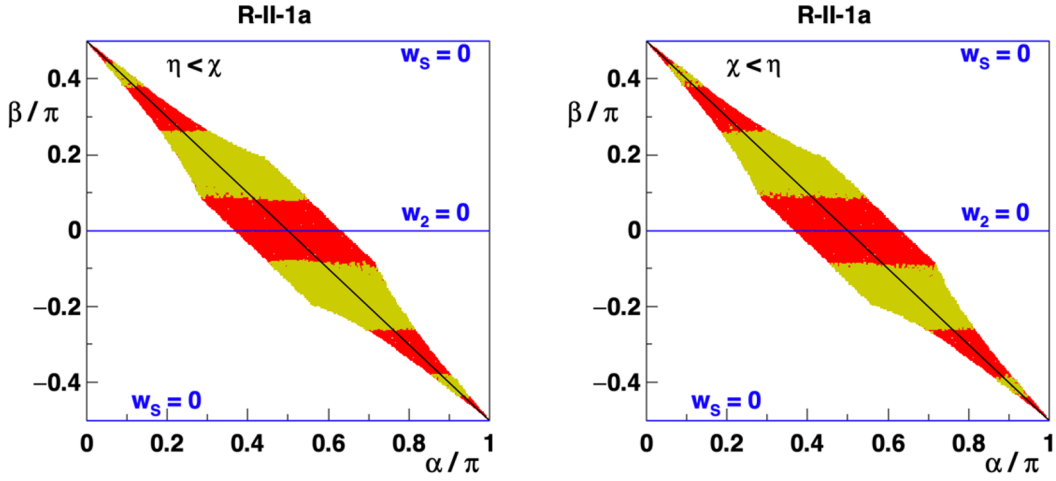

Figure 3. Constraints on α and β from the gauge and Yukawa couplings. We take $\beta \in [-\frac{\pi}{2},\ \frac{\pi}{2}]$ and $\alpha \in [0,\ \pi]$, see also eq. (4.35). The white region is excluded. The black diagonal line identifies the SM-like limit, which is $\alpha + \beta = \pi/2$. The coloured regions are compliant with Cut 1, whereas the yellow regions are also compliant with Cut 2 constraints. Values of β for which w_2 or w_S vanish are identified.

5.2 The SM-like limit

The Standard Model like limit refers to the limit in which the CP even boson, which is in the only doublet that acquires vev when going to the Higgs basis, is already a physical boson, i.e., a mass eigenstate and therefore, does not mix with the other neutral scalars. This doublet is the one that contains the would-be Goldstone bosons $G^{\pm}$ and G^0. This limit is special and is referred to as the SM-like limit because this CP even neutral boson behaves in many aspects as the SM boson. This limit is reached for $\sin(\alpha+\beta) = 1$ ($\alpha = -\beta + \pi/2$) as stated before. In this case we see from eq. (4.36a) that only h has couplings of the type VVH and their strengths coincide with those of the SM. Furthermore, from the fact that h is in the only doublet that acquires vev we see that in this limit h couples to the fermions with the same strength as the SM Higgs boson. In fact, this can be seen from eq. (4.39), since in this limit $\sin\alpha = \cos\beta$.

We shall adopt the following 3-σ bounds from the PDG [95]:

$$\kappa_{VV}^2 \equiv |\sin(\alpha+\beta)|^2 \in \{1.19 \pm 3\,\sigma\}, \qquad \text{which comes from } h_{\rm SM}W^+W^-, \tag{5.3a}$$

$$\kappa_{ff}^2 \equiv \left|\frac{\sin\alpha}{\cos\beta}\right|^2 \in \{1.04 \pm 3\,\sigma\}, \qquad \text{which comes from } h_{\rm SM}\bar{b}b. \tag{5.3b}$$

Note that we must impose the same sign for these two couplings of eq. (5.3), in order not to spoil the interference required for $h_{\rm SM} \to \gamma\gamma$.

5.3 Electroweak precision observables

The electroweak oblique parameters are specified by the S, T, and U functions. Sufficient mass splittings of the extended electroweak sector can account for a non-negligible

JHEP01(2022)120

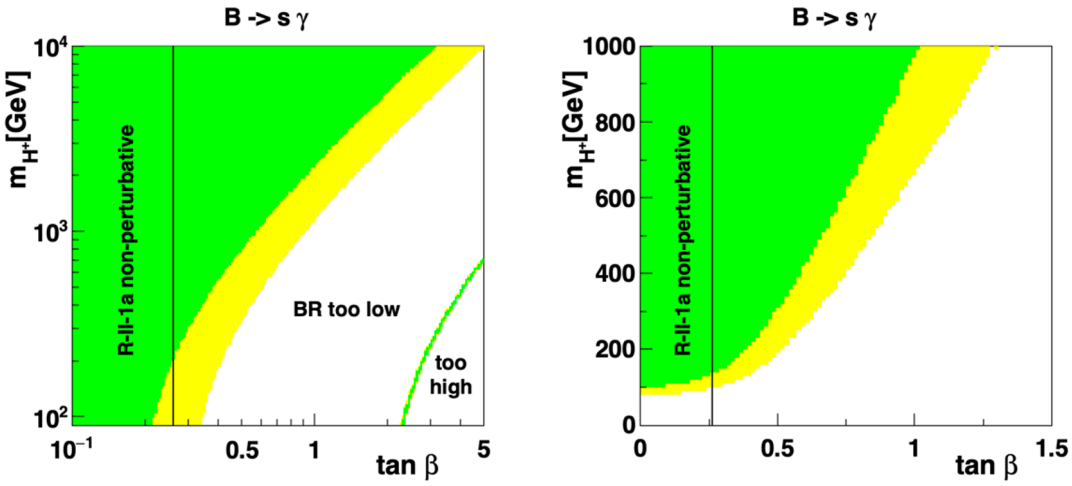

Figure 4. Regions in the $\tan\beta$–m_{H^+} plane that survive the $\bar{B} \to X(s)\gamma$ constraint. Left: logarithmic representation out to larger $\tan\beta$ and m_{H^+}. Right: linear representation of the small-$\tan\beta$ region. The yellow region accommodates a 3-σ tolerance with respect to the experimental rate, whereas in the green regions, the models are within a 2-σ bound. The vertical line at $\tan\beta = 0.26$ is the lower bound on $|\tan\beta|$ compatible with $|\lambda_4| < 4\pi$ for R-II-1a.

contribution. The S and T parameters get the most sizeable contributions. Results are compared against the experimental constraints provided by the PDG [95], assuming that $U = 0$. The model-dependent rotation matrices, needed to evaluate the set of S and T, are presented in appendix C.2.

5.4 B physics constraints

The importance of a charged scalar exchange for the $\bar{B} \to X(s)\gamma$ rate has been known since the late 1980's [96–98]. The rate is determined from an expansion of the relevant Wilson coefficients in powers of $\alpha_s/(4\pi)$, starting with (1) the matching of these coefficients to the full theory at some high scale ($\mu_0 \sim m_W$ or m_t), then (2) evolving them down to the low scale $\mu_b \sim m_b$ (in this process the operators mix), and (3) determine the matrix elements at the low scale [99–112].

We here follow the approach of Misiak and Steinhauser [113]. While the considered S_3-based models have two charged Higgs bosons, only one couples to fermions. This implies that we may adopt the approach used for the 2HDM with relative Yukawa couplings of the active charged scalar, eq. (4.41) (in the notation of ref. [113]),

$$A_u = A_d = \tan\beta. \tag{5.4}$$

We show in figure 4 the regions in the $\tan\beta$-m_{H^+} parameter plane that are not excluded by this constraint. The situation is quite different from that of the more familiar 2HDM with Type II Yukawa couplings. According to eq. (5.4) the relevant couplings are the same as those of the 2HDM Type I model, with the exception that we are here interested in *small*

JHEP01(2022)120

values of $\tan\beta$. While the $\bar{B} \to X(s)\gamma$ constraint excludes large values of $\tan\beta$, low values are for R-II-1a also cut off due to the perturbativity constraint, we have $|\tan\beta| \gtrsim 0.26$, as discussed in section 5.1.

Since $A_u A_d > 0$, there is a region of negative interference between the SM-type contributions and the loop with the charged Higgs: as we increase the value of $\tan\beta$ for fixed m_{H^+}, the branching ratio will first diminish, and then at some point come back up, as illustrated in the lower right-hand corner of the left panel of figure 4. This interference region is ruled out by Cut 3. For any fixed value of $\tan\beta$, on the other hand, for sufficiently high mass m_{H^+}, the rate approaches the SM value.

We adopt the experimental value, $\mathrm{Br}\left(\bar{B} \to X(s)\gamma\right) \times 10^4 = 3.32 \pm 0.15$ [95] and impose an $(n = 3)$-σ tolerance, together with an additional 10 per cent computational uncertainty,

$$\mathrm{Br}\left(\bar{B} \to X(s)\gamma\right) \times 10^4 = 3.32 \pm \sqrt{(3.32 \times 0.1)^2 + (0.15\, n)^2}\,. \tag{5.5}$$

The acceptable region, corresponding to the 3-σ bound, is [2.76; 3.88].

5.5 LHC Higgs constraints

We require that the Higgs-like particle, h, full width is within $\Gamma_h = 3.2^{+2.8}_{-2.2}\,\mathrm{MeV}$, which is an experimental bound adopted from [95]. In the SM the total width of the Higgs boson is around 4 MeV. The upper value, i.e., $\Gamma_h = 6$ MeV is used in preliminary checks within the spectrum generator.

5.5.1 Decays $h \to \gamma\gamma$ and $h \to gg$

The di-photon partial decay width is modified by the charged-scalar loop in comparison to the SM case. The one-loop width is known [2, 114, 115]:

$$\begin{aligned}\Gamma\left(h \to \gamma\gamma\right) = \frac{\alpha^2 m_h^3}{256\pi^3 v^2}\Bigg| \sum_f Q_f^2 N_c C^S_{ffh} \mathcal{F}^S_{1/2}\left(\tau_f\right) + C_{W^+W^-h}\mathcal{F}_1\left(\tau_{W^\pm}\right) \\ + \sum_{\varphi_i^\pm} C_{\varphi_i^+\varphi_i^- h}\mathcal{F}_0\left(\tau_{\varphi^\pm}\right)\Bigg|^2,\end{aligned} \tag{5.6}$$

where α is the fine-structure constant, Q_f is the electric charge of the fermion, $N_c = 3\,(1)$ for quarks (leptons), and the C's are the couplings normalised to those of the SM,

$$\mathcal{L}'_{\mathrm{int}} = -\frac{m_f}{v} C^S_{\bar{f}fh}\bar{f}fh + g m_W C_{W^+W^-h} W^+_\mu W^{\mu-} h - \frac{2m^2_{\varphi_i^\pm}}{v} C_{\varphi_i^+\varphi_i^- h}\varphi_i^+\varphi_i^- h. \tag{5.7}$$

The spin-dependent functions $\mathcal{F}^S_{1/2}$, $\mathcal{F}_1$, and $\mathcal{F}_0$ can be found in appendix C. Contributions from the fermionic loop and gauge loop versus the charged scalar loop are presented in figure 5.

In the SM case, the dominant Higgs production mechanism is through gluon fusion. However, due to experimental limitations we do not explicitly consider constraints on this channel. The rate for the two-gluon decay at the leading order is [116–119]

$$\Gamma\left(h \to gg\right) = \frac{\alpha_S^2 m_h^3}{128\pi^3 v^2}\left|\sum_f C^S_{\bar{f}fh}\mathcal{F}^S_{1/2}(\tau_f)\right|^2, \tag{5.8}$$

JHEP01(2022)120

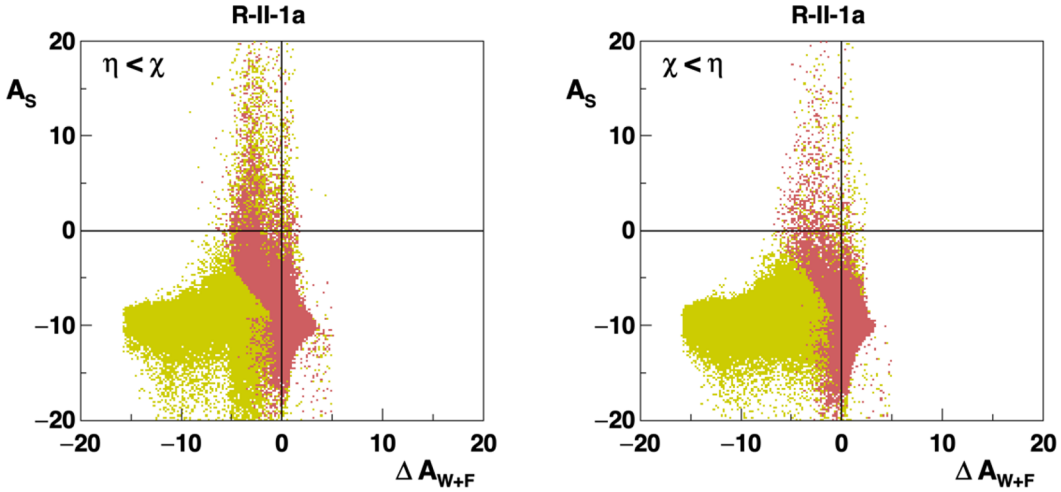

Figure 5. Scatter plots of additional contributions to the di-photon decay amplitudes, normalised to the SM value, expressed in per cent. Complex numbers arise from the spin-dependent function $\mathcal{F}^S_{1/2}$ of equation (C.1b) for fermions lighter than the Higgs-like particle h. The $A_{\rm S}$ value represents the normalised contribution from the charged scalar loop, $A_{\rm S}/|A_{\rm SM}|$, while the $\Delta A_{\rm W+F}$ value stands for an additional contribution to the SM-like part due to the W and fermion loops, $\Delta A_{\rm W+F} = (|A_{\rm W+F}| - |A_{\rm SM}|)/|A_{\rm SM}|$. Yellow dots represent parameters surviving Cut 2, while the red ones represent those surviving also LHC Higgs-particle constraints: full width, the invisible branching ratio, and the di-photon constraint.

where α_S is the strong coupling constant. The decay width of this process can be enhanced or diminished with respect to the SM case. Such behaviour is caused by an additional factor for the amplitude, $g^{\text{R-II-1a}}_{\bar{f}fh} = g^{\rm SM}_{\bar{f}fh} \sin\alpha/\cos\beta$.

The normalised two-gluon branching ratio to the SM case is depicted in figure 6. The gluon branching ratio for DM mass below $m_h/2$ can become low due to the opening of the invisible channel, $h \to \varphi_i\varphi_i$. However, such cases are partially excluded by other LHC Higgs-particle constraints of Cut 3. Even with more experimental data collected, the two-gluon constraint will not play a very significant role in terms of constraining the R-II-1a model. Most of the two-gluon points are within the range $\mu_{gg} \in [0.9, 1.1]$.

In light of the above discussion, we do not aim to account for the correct h two-gluon production factor and approximate the di-photon channel strength to be

$$\mu_{\gamma\gamma} \approx \frac{\Gamma(h \to \gamma\gamma)}{\Gamma^{\rm exp}(h \to \gamma\gamma)} \frac{\Gamma^{\rm exp}(h)}{\Gamma(h)}, \tag{5.9}$$

with $\mu_{\gamma\gamma} = 1.11 \pm 0.10$ [95]. We evaluate this constraint allowing for an additional 10 per cent computational uncertainty, and impose an $(n = 3)$-σ tolerance,

$$\mu_{\gamma\gamma} = 1.11 \pm \sqrt{(1.11 \times 0.1)^2 + (0.1n)^2}, \tag{5.10}$$

which corresponds to the 3-σ range of [0.79; 1.43].

JHEP01(2022)120

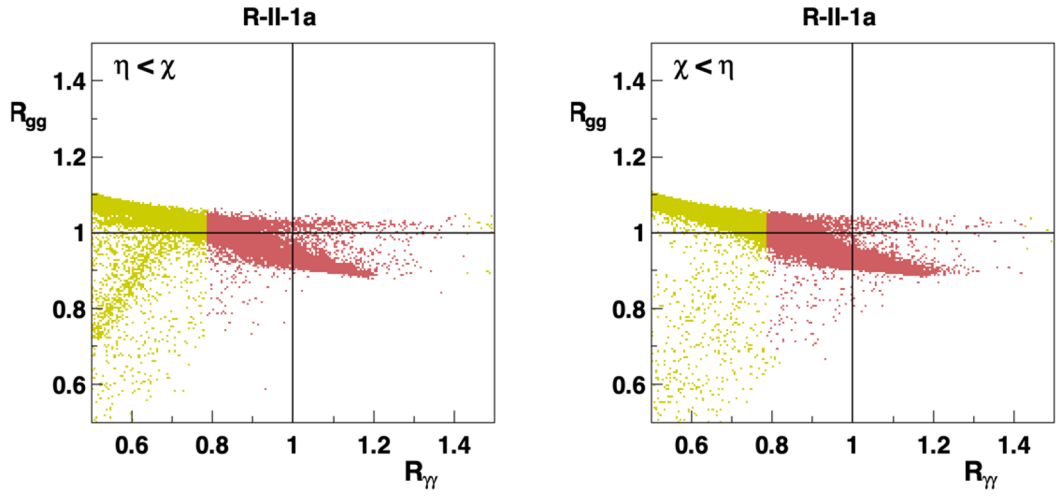

Figure 6. Two-gluon versus di-photon Higgs-like particle branching ratios, normalised to the SM value, $R_{ii} \equiv \mathrm{Br}(h \to ii)/\mathrm{Br}^{\mathrm{SM}}(h \to ii)$, for different R-II-1a mass orderings. The black lines represent the SM case. A proper evaluation of the di-photon channel (5.9) would require an additional factor from the two-gluon channel arising from the h production, i.e., each point would have to be scaled by multiplying both of the values presented in the plot, $\mu_{\gamma\gamma} = R_{gg}R_{\gamma\gamma}$. Points above the $R_{gg} = 1$ line would shift right, while those below would shift left.

5.5.2 Invisible decays, $h \to$ inv.

The SM-like Higgs boson can decay to the lighter scalars $h \to \varphi_i\varphi_j$ provided $2m_{\varphi_i} < m_h$. If the decays are kinematically allowed, these processes can enhance the total width of the SM-like Higgs state sizeably. The observed upper limit of the invisible Higgs branching ratio reported by LHC at 95% CL is

$$\mathrm{Br}\,(h_{\mathrm{SM}} \to \mathrm{inv.}) < 26\%, \text{ by ATLAS [120]}, \tag{5.11a}$$

$$\mathrm{Br}\,(h_{\mathrm{SM}} \to \mathrm{inv.}) < 19\%, \text{ by CMS [121]}. \tag{5.11b}$$

The decay width of h into a pair of scalars φ_i is given by

$$\Gamma\,(h \to \varphi_i\varphi_j) = \frac{2-\delta_{ij}}{32\pi m_h^3}\left|g_{h\varphi_i\varphi_j}\right|^2 \sqrt{\left[m_h^2 - \left(m_{\varphi_i} + m_{\varphi_j}\right)^2\right]\left[m_h^2 - \left(m_{\varphi_i} - m_{\varphi_j}\right)^2\right]}, \tag{5.12}$$

with a symmetry factor $(2-\delta_{ij})$, where δ_{ij} is the Kronecker delta. The appropriate trilinear couplings are given by equations (A.2a) and (A.2c). In appendix A the overall factor of "$-i$" is left out.[2] Due to CP conservation there is no coupling $g\,(h\,\eta\,\chi)$, therefore the Higgs-like particle can decay only into pairs of inert neutral scalars,

$$\Gamma\,(h \to \varphi_i\varphi_i) = \frac{1}{32\pi m_h^2}\left|g_{h\varphi_i\varphi_i}\right|^2 \sqrt{m_h^2 - 4m_{\varphi_i}^2}. \tag{5.13}$$

[2]We use the notation $g_{\ldots} = -ig(\ldots)$.

JHEP01(2022)120

These are the only two possible channels ($h \to \eta\eta$ and $h \to \chi\chi$) which can contribute to the invisible decay. Channels with other scalars are kinematically inaccessible due to the assumed limits, i.e., mass ordering and LEP constraints.

The experimental bounds can be applied directly if there is only a single channel open. However, there is a possibility that both inert neutral states, η and χ, can be kinematically accessible. In a simplistic approximation a particle escapes a detector of 30 meters, assuming no time dilation factor, if its lifetime exceeds a value of $\tau \gtrsim 10^{-7}$ seconds. The value can be expressed in terms of the total decay width, $\Gamma^{\rm tot} \lesssim 6.6 \times 10^{-18}\,\text{GeV}$. Based on the total width of the next-to-lightest state, φ_j, two situations are possible:

- If the particle is not long-lived, $\Gamma^{\rm tot}(\varphi_j) > 6.6 \times 10^{-18}\,\text{GeV}$, it will decay within the detector through $h \to \varphi_j\varphi_j \to \varphi_i\varphi_i Z^* Z^*$, with the Z^* subsequently also decaying. In this case only the $h \to \varphi_i\varphi_i$ channel will contribute to $\text{Br}\,(h \to \text{inv.})$.

- When $\Gamma^{\rm tot}(\varphi_j) < 6.6 \times 10^{-18}\,\text{GeV}$, the invisible branching ratio will be given by

$$\text{Br}\,(h \to \text{inv.}) = \frac{\Gamma\,(h \to \eta\eta) + \Gamma\,(h \to \chi\chi)}{\Gamma\,(h)}. \tag{5.14}$$

In the R-II-1a model we found that the decay rate of the next-to-lightest inert neutral particle is way above $\Gamma = \mathcal{O}(10^{-18})\,\text{GeV}$. In our calculations we shall adopt the PDG [95] constraint, which is $\text{Br}^{\rm exp}\,(h \to \text{inv.}) < 0.19$.

5.6 The h scalar self interactions

Let us next consider the trilinear and quadrilinear self interactions, given by eqs. (A.1a) and (A.4b). The SM Higgs self-interactions are [122]

$$g(h^3_{\rm SM}) = \frac{3m^2_{h_{\rm SM}}}{v}, \quad g(h^4_{\rm SM}) = \frac{1}{v} g(h^3_{\rm SM}). \tag{5.15}$$

In the R-II-1a model, these couplings can be expanded in terms of m_h^2, m_H^2 and m_η^2,

$$g(h^3) = \frac{3m_h^2}{v}\left[\sin(\alpha+\beta) + \frac{2\cos^2(\alpha+\beta)\cos(\alpha-\beta)}{\sin(2\beta)}\right] + \frac{2m_\eta^2\cos^3(\alpha+\beta)}{3v\sin(2\beta)\cos^2(\beta)}, \tag{5.16a}$$

$$\begin{aligned} g(h^4) = {} & \frac{3m_h^2}{v^2}\left[\sin(\alpha+\beta) + \frac{2\cos^2(\alpha+\beta)\cos(\alpha-\beta)}{\sin(2\beta)}\right]^2 \\ & + \frac{3m_H^2\cos^2(\alpha+\beta)\sin^2(2\alpha)}{v^2\sin^2(2\beta)} + \frac{2m_\eta^2\cos^3(\alpha+\beta)\left[3\cos(\alpha)\cot(\beta)+\sin(\alpha)\right]}{3v^2\sin(2\beta)\cos^3(\beta)}. \end{aligned} \tag{5.16b}$$

After imposing $\alpha + \beta = \pi/2$ we arrive at the SM-like Higgs couplings.

In the future, the trilinear Higgs self interactions may become a crucial test for new physics. For this purpose, we show in figure 7 the h trilinear coupling, relative to the SM value.

JHEP01(2022)120

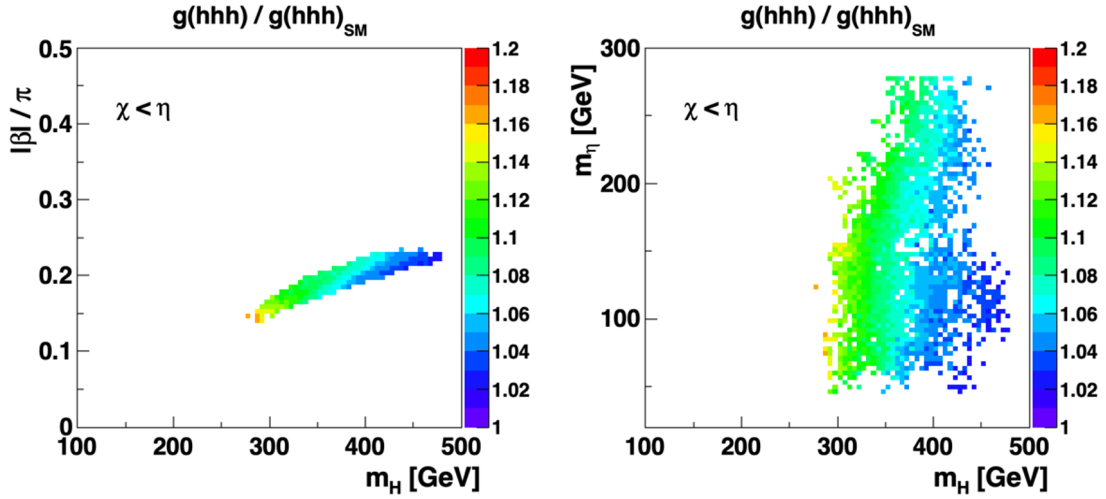

Figure 7. Trilinear self interactions of the Higgs-like particle normalised to the SM value, after applying Cut 3, represented by the coloured bar. The coupling is presented as a function of the mass of the heavier CP-even state m_H and the Higgs basis rotation angle β (left) or the mass of the neutral inert scalar m_η (right).

5.7 Astrophysical observables

We consider a standard cosmological model with a freeze-out scenario. The cold dark matter relic density along with the decay widths discussed above and other astrophysical observables are evaluated using micrOMEGAs 5.2.7. The 't Hooft-Feynman gauge is adopted, and switches are set to default values VZdecay = VWdecay = 1, identifying that 3-body final states will be computed for annihilation processes only. The fast = −1 switch identifies that very accurate calculation is used. The steering CalcHEP [123] model files are produced with the help of SARAH [124, 125].

We shall adopt the cold dark matter relic density value of 0.1200 ± 0.0012 taken from PDG [95]. The relic density parameter will be evaluated using a 3-σ tolerance and assuming an additional 10 per cent computational uncertainty,

$$\Omega h^2 = 0.1200 \pm \sqrt{(0.1200 \times 0.1)^2 + (0.0012\, n)^2}\,, \tag{5.17}$$

corrponding to the [0.1075; 0.1325] region.

Let us recall results of figure 1. In the IDM, two regions compatible with the cold dark matter relic density were identified. These correspond to the high-mass region and the intermediate-mass region. The high-mass region is in agreement with the relic density due to two factors:

- Near-mass-degeneracy among the scalars of the inert sector. Small mass splittings correspond to tiny couplings, and different inert-scalar contributions to the annihilation will be suppressed and result in an acceptable relic density;

JHEP01(2022)120

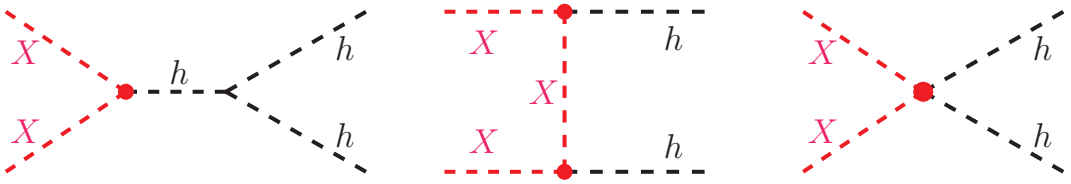

Figure 8. Feynman diagrams contributing to XX (particles of the inert sector) annihilation channels at high DM masses.

- Freedom to choose the Higgs boson portal coupling λ_L. This parameter controls the trilinear XXh and quartic $XXhh$ coupling, and must be sufficiently small. Here, X refers to scalars of the inert sector, both charged and neutral.

In this region, the main DM annihilation is into W^+W^-. However, the relic density can be maintained at an acceptable level by suppressing annihilation via an intermediate h boson and into a pair of h bosons, illustrated in figure 8. The desired relic abundance can be achieved by adjusting the mass splittings.

Whereas the IDM and the 3HDMs considered in figure 1 have an adjustable portal coupling (often referred to as λ_L for the IDM), the present model is constrained by the underlying S_3 symmetry. Here, there is not a single portal coupling, but two: a trilinear XXh and a quartic $XXhh$, plus additional ones involving other scalars. Furthermore, these are not "free", but correlated with other features of the model. In particular, they are constrained by the scalar masses and two angular parameters, α and β.

Let us consider a simplified picture with heavy active scalar bosons. At high DM masses the main DM annihilation channel is into W^+W^-. This channel is controlled by the gauge coupling. In addition, channels leading to h scalars will be accessible, as illustrated in figure 8. These amplitudes are controlled by the portal couplings which should be constrained, since otherwise the DM relic density becomes too low.

To first order in δ (in the neighbourhood of the SM-like limit), where $\alpha = \pi/2 - \beta + \delta$, the behaviour of the portal couplings is quite simple. In the limit of $\delta \to 0$ we arrive at

$$\frac{g(XXh)}{v} = g(XXhh) = \frac{1}{v^2}\left[m_h^2 + 2m_X^2\right]. \tag{5.18}$$

This relation shows that the portal couplings will grow with increasing DM mass.

Values of the trilinear and quartic couplings are shown in figure 9. As shown in this figure, the correlation with DM mass (5.18) is qualitatively borne out by the parameter points surviving Cut 2.

In the aforementioned simplification we argued that there are no good DM candidates for high mass values. In the full R-II-1a model other annihilation channels involving active scalars are also accessible. For example, there is a contribution from the H scalar to the $X\,X \to h\,h$ process through the s-channel. Furthermore, there are other accessible active-inert scalar channels. This explains why the DM relic density is saturated at $\Omega h^2 = \mathcal{O}(10^{-4})$ at high DM values, see figure 10.

Going down in the DM mass, the situation changes as follows. At around $m_{\varphi_i} \approx 200\,\text{GeV}$ there is a kink and the maximal relic density increases from $\Omega h^2 = \mathcal{O}(10^{-4})$ up

JHEP01(2022)120

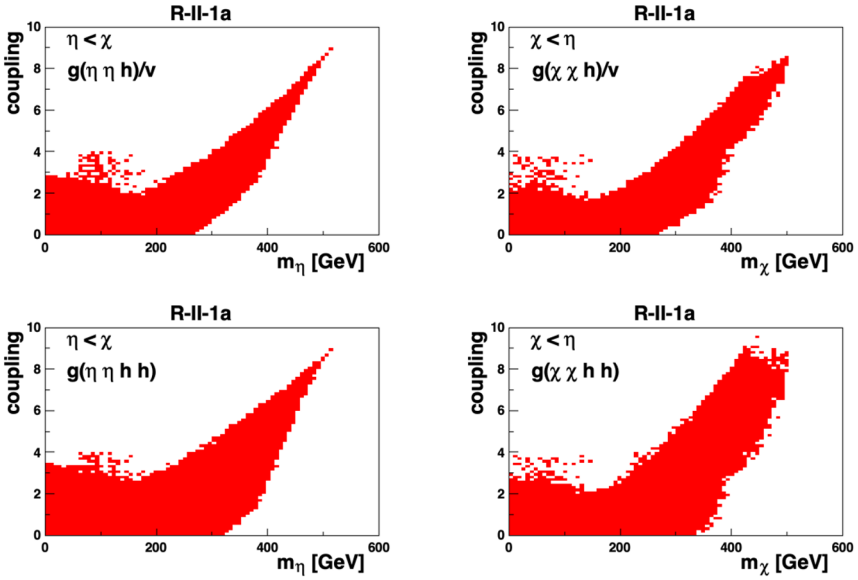

Figure 9. Absolute value of the trilinear portal coupling $|g(XXh)/v|$ (top) and the quartic portal coupling $|g(XXhh)|$ (bottom) versus the lightest inert particle mass.

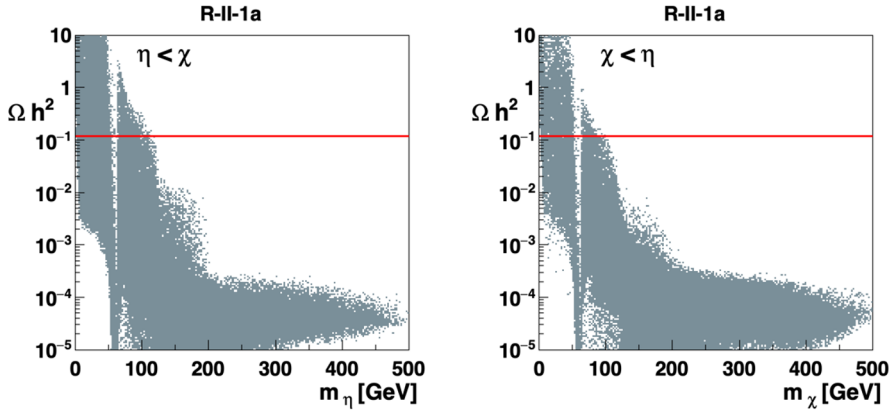

Figure 10. Dark matter relic density for the R-II-1a model. The region compatible with the observed DM relic density does not allow for masses above around 120 GeV. In the high-mass region, $m_{\varphi_i} \gtrsim 500$ GeV, the DM relic density is shown to be too low.

to $\Omega h^2 = \mathcal{O}(10^{-2})$. In this range, the main annihilation (or loss) mechanisms are via the channels $\varphi_i\varphi_i \to hh$ and $\varphi_i\varphi_i \to W^\pm W^\mp$. In this same mass region many parameter points also yield $\Omega h^2 < \mathcal{O}(10^{-4})$. This happens when the dominant annihilation channels are $\varphi_i\varphi_i \to AZ$ and $\varphi_i\varphi_i \to H^\pm W^\mp$, through either h or H in the s-channel, or via φ_j or $h^\pm$ (based on quantum numbers) in the t-channel.

Then, in the mass region $m_{\varphi_i} \in [m_h/2,\ 120\ \text{GeV}]$, the relic density ranges from above unity down to below $\Omega h^2 = \mathcal{O}\left(10^{-5}\right)$. The main annihilation channels are into a pair of (virtual) $W^\pm$ bosons or b-quarks, with the latter becoming increasingly important as the

JHEP01(2022)120

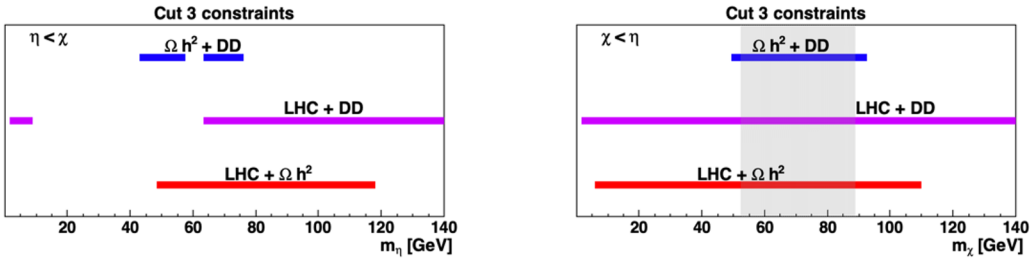

Figure 11. Allowed mass regions of the DM candidate involving different Cut 3 constraints. Blue: relic density satisfied together with direct detection. Purple: LHC Higgs constraints along with direct detection constraints. Red: relic density and LHC Higgs constraints. Grey: all of the Cut 3 constraints are satisfied. Note that additional input parameters are not shown.

DM mass decreases. However, there are also cases when the dominant annihilation channel is $\varphi_i\varphi_i \to gg$, which can contribute more than 50%.

Finally, in the DM mass region corresponding to values below $m_h/2$, the primary annihilation or loss mechanism is $\varphi_i\varphi_i \to b\bar{b}$ trough a virtual h. This channel depends critically on the portal, i.e., the trilinear coupling $g(\varphi_i\varphi_i h)$.

6 Cut 3 discussion

It is convenient to discuss the low-mass DM situation in terms of the following four critical constraints:

- a (Ωh^2): DM relic density, eq. (5.17);
- b (LHC): h invisible branching ratio and $\Gamma_h \leq 6\,\text{MeV}$;
- c (LHC): h di-photon rate, eq. (5.10);
- d (DD): DM direct detection.

6.1 The η case

For the case when the η scalar is the lightest ("η case"), from figure 10 it looks as if there could be solutions for the range of $m_\eta \in [2, 120]$ GeV. However, in the low-mass range of this interval, the h invisible branching ratio, together with the relic DM density constraint becomes incompatible with the experimental data. In light of this fact, in the remainder of the discussion presented in this paragraph we shall focus on η masses up to 120 GeV since we already know that criterion (a) excludes higher masses. Both constraints, i.e., (a) and (b), alongside with Cut 1 and Cut 2, are satisfied within the region $m_\eta \in [40, 120]$ GeV. The final checks are then the di-photon (c) and the direct detection constraints (d). These two constraints are very severe and eliminate a large region of the parameter space. When imposed separately, the strongest constraint comes from the direct detection criteria, which are satisfied in the mass region $m_\eta \in [43, 120]$ GeV and at values below $m_\eta \lesssim 10$ GeV.

We list different Cut 3 paired constraints in figure 11 after imposing cuts 1 and 2. We work with 8 input parameters, 6 masses and 2 angles. After imposing Cut 3, there

JHEP01(2022)120

will be different domains allowed by each of the three checks, Ωh^2, DD, or LHC, imposed separately. The intersection of all these domains would correspond to Cut 3 being satisfied. Figure 11 shows the allowed mass regions of the DM candidate after imposing two of the different checks at a time. Overlapping lines do not guarantee that there are regions of parameters satisfying all of the constraints simultaneously since there are seven more parameters to consider. There is no region for either (Ωh^2+DD) or (LHC+DD) satisfied for $m_\eta \approx m_h/2$. In fact, for the η case we found no parameter point satisfying all of the Cut 3 constraints simultaneously.

6.2 The χ case

For the case when the χ scalar is the lightest ("χ case"), the Ωh^2 distribution is slightly shifted towards lower relic density values, as shown in figure 10. As a result, the region compatible with the relic density is $m_\chi \in [2, 105]$ GeV. For the η case with masses below 40 GeV, when the (b) constraint is imposed, all Ωh^2 are above 0.22. This does not apply to the χ case since in this case Ωh^2 can go as low as ≈ 0.07. Nevertheless, the sub-40 GeV region is not compatible with Cut 3. However, the region $m_\chi \in [52.5, 89]$ GeV survives cuts 1 to 3 when applied simultaneously. The lower DM mass range is compatible with other models presented in figure 1, while slightly heavier DM candidates are also allowed within the R-II-1a framework. When applied simultaneously, conditions (a) and (d) are satisfied for a broader range of $m_\chi \in [45.5, 92]$ GeV. Bounds from pairs of different Cut 3 checks are shown in figure 11.

It is instructive to see which points within the parameter range survive all the cuts. The mass scatter plots of Cut 3 superimposed on the Cut 2 points are given in figure 12. There are no solutions with active neutral states being degenerate. Moreover, these masses reach at most $m_A^{\max} \sim 340$ GeV and $m_H^{\max} \sim 450$ GeV. The CP-odd state, A, can be as light as the observed SM-like Higgs boson, $m_A \simeq m_h$. On the other hand, such low masses for the H boson are disfavoured by Cut 3. The charged bosons that survive Cut 3 are also light, with $m_{H^\pm}^{\max} \sim 460$ GeV and $m_{h^\pm}^{\max} \sim 310$ GeV. It is interesting to note that the charged active scalar can be as light as $m_{H^\pm}^{\min} \sim 177$ GeV. Future experimental data on the decays of the charged bosons will be useful to test the model. For the B physics constraints we applied only the indirect experimental bounds on the $\bar{B} \to X(s)\gamma$ rate, however other channels might lead to stronger constraints on the mass of the $H^\pm$ scalar. Finally, as noted earlier we have for the DM candidate $m_\chi \in [52.5, 89]$ GeV and the other inert neutral state, η, can be as heavy as $m_\eta^{\max} \sim 310$ GeV. It is also interesting to note that either η or $h^\pm$ can be the next-lightest member of the inert doublet.

In addition to the mass parameters, angles are also used as input. The allowed ranges in the α - β plane are shown in figure 13. The solutions satisfying all cuts are asymmetrically distributed along the black diagonal line, which represents the SM-like limit. In the right panel of figure 13 we also show the gauge (κ_{VV}) and Yukawa (κ_{ff}) couplings, relative to the SM values, see eqs. (5.3). Figure 13 shows that the experimental data are more stringent for κ_{ff} than for κ_{VV}. The lack of symmetry in the distribution of the grey points with respect to the diagonal, corrresponding to the SM-like limit, in the left panel translates into a significant population of κ_{ff}-values below unity in the right panel.

JHEP01(2022)120

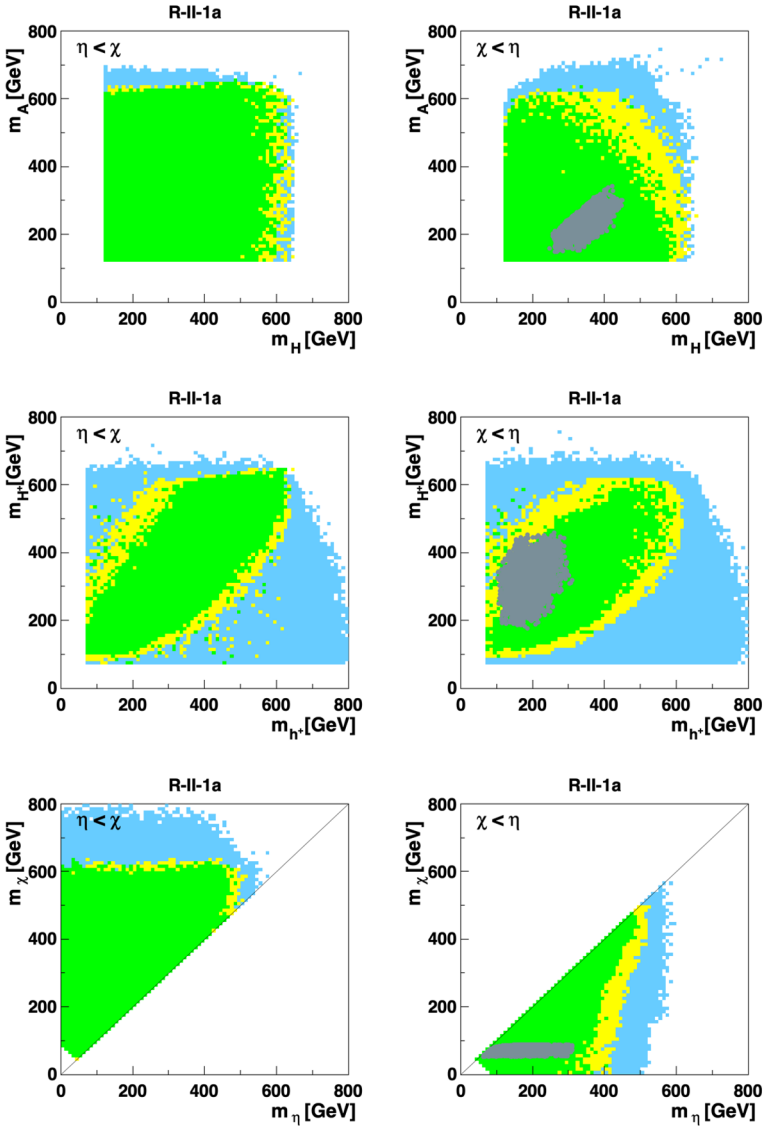

Figure 12. Scatter plots of masses that satisfy different cuts, for both orderings of η and χ. Identical notation as in figure 2. The light-blue region satisfies Cut 1 and accommodates the 16π unitarity constraint. The yellow region accommodates a 3-σ tolerance with respect to Cut 2, whereas in the green regions, the model is within the 2-σ bound of these values. The grey points are compatible with all cuts and are only present in the right-hand panels.

JHEP01(2022)120

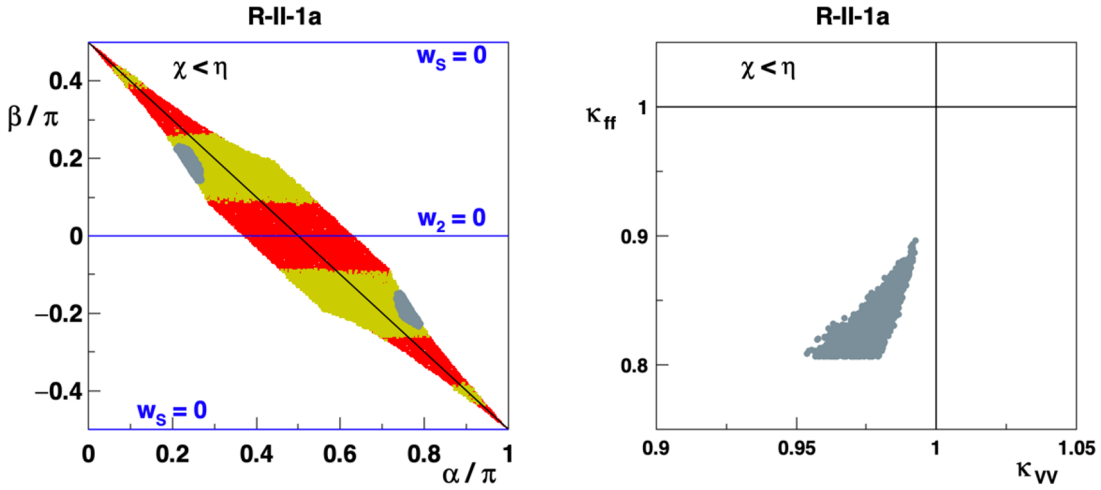

Figure 13. Left: constraints on α and β from the gauge and Yukawa couplings. Identical colour convention and notation as in figure 3. The superimposed grey points also satisfy the Cut 3 constraints for the χ case. Right: corresponding constraints on relative Yukawa κ_{ff} and gauge couplings κ_{VV} with respect to the SM.

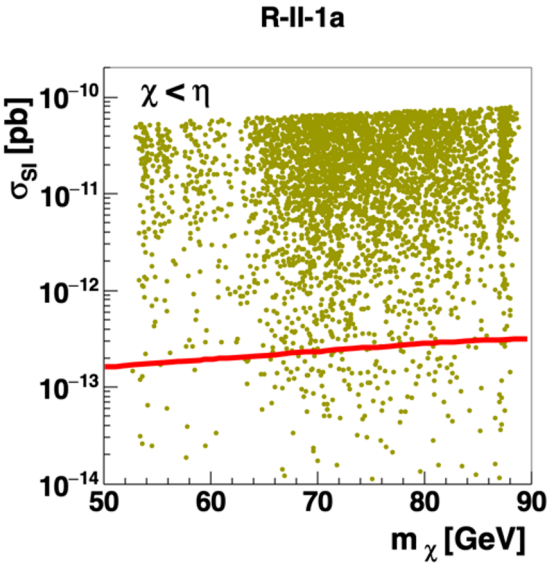

Figure 14. The spin-independent DM-nucleon cross section compatible with XENON1T [77] data at 90% C.L. The points represent Cut 3 satisfied for the χ DM case. The red line corresponds to an approximate neutrino floor, which can be defined in various ways.

We present direct detection constraints in figure 14. We note that in practically the whole mass range there are parameter points at lower cross sections. Thus, a future improvement on this direct detection constraint is not obviously going to reduce the range of masses allowed by the model.

Finally, in table 2 we show some benchmarks.

JHEP01(2022)120

Parameter	BP 1	BP 2	BP 3	BP 4	BP 5	BP6	BP7	BP8	BP9
DM (χ) mass [GeV]	52.6	56.1	59.6	63.02	65.7	70.3	75.0	82.2	88.6
η mass [GeV]	62.7	203.8	270.4	169.4	150.5	157.7	202.8	127.8	210.7
h^+ mass [GeV]	115.4	167.4	273.6	188.6	214.1	170.5	232.0	151.8	243.0
H^+ mass [GeV]	192.6	369.5	367.4	246.6	265.5	405.8	319.8	410.6	311.9
H mass [GeV]	263.9	349.3	352.9	276.3	298.2	402.0	368.5	405.2	317.6
A mass [GeV]	179.2	208.0	190.7	173.9	205.2	255.3	251.3	330.0	247.0
β/π	0.162	-0.204	-0.201	-0.165	0.163	0.220	0.203	-0.218	0.183
α/π	0.252	0.763	0.765	0.752	0.254	0.225	0.239	0.769	0.238
$\sigma_{\rm SI}$ [10^{-11} pb]	0.029	1.456	4.928	0.176	5.326	1.341	2.711	8.553	4.491
$\eta \to \chi q\bar{q}$ [%]	63.27				54.38	54.35		53.95	
$\eta \to \chi b\bar{b}$ [%]	0.48				14.80	14.85		13.90	
$\eta \to \chi \nu\bar{\nu}$ [%]	24.62				20.48	20.46		20.72	
$\eta \to \chi l\bar{l}$ [%]	11.61				10.33	10.33		11.42	
$\eta \to \chi Z$ [%]		99.98	53.09	100			100		100
$\eta \to \chi A$ [%]			46.91						
$h^+ \to \chi W^+$ [%]		100	100	99.98	99.89	99.99	99.99		99.99
$h^+ \to \eta q\bar{q}$ [%]	20.18							0.30	
$h^+ \to \eta \nu\bar{l}$ [%]	9.88							0.16	
$h^+ \to \chi q\bar{q}$ [%]	46.94							66.82	
$h^+ \to \chi \nu\bar{l}$ [%]	22.99							32.71	
$H^+ \to t\bar{b}$ [%]	9.07	43.69	58.23	95.09	95.78	30.95	96.25	31.54	93.59
$H^+ \to AW^+$ [%]		20.56	35.74	0.29	0.06	8.66	0.05	0.05	0.05
$H^+ \to hW^+$ [%]		1.94	2.67	4.46	4.00	1.23	2.86	1.15	6.20
$H^+ \to h^+\eta$ [%]	85.9					43.74		61.68	
$H^+ \to h^+\chi$ [%]	5.00	33.74	3.26			15.36	0.68	5.53	
$H \to \chi\chi$ [%]	0.15	0.03	0.07	0.87	15.03		11.34	7.63	63.75
$H \to \eta\eta$ [%]	89.9					24.89		25.31	
$H \to hh$ [%]	3.07	2.64	9.40	34.59	33.53	1.33	13.43	0.88	14.72
$H \to AZ$ [%]	0.09	13.55	70.93	13.91	2.87	7.61	22.78		0.07
$H \to W^+W^-$ [%]	4.06	3.13	10.40	34.98	33.35	1.89	16.32	1.26	14.70
$H \to ZZ$ [%]	1.75	1.43	4.77	15.29	14.82	0.88	7.53	0.59	6.62
$H \to h^+h^-$ [%]	0.80	78.59				52.94		56.33	
$H \to q\bar{q}$ [%]		0.62	4.40	0.32	0.34	10.43	28.52	8.00	0.12
$A \to \eta\chi$ [%]	99.97					99.32		99.01	
$A \to b\bar{b}$ [%]	0.02	79.78	84.15	84.63	75.28	0.07	8.84	0.02	4.76
$A \to q\bar{q}$ [%]		3.56	3.75	3.77	3.36		0.39		0.21
$A \to \tau^+\tau^-$ [%]		9.85	10.19	10.00	9.24		1.13		0.61
$A \to hZ$ [%]		6.81	1.87	1.55	12.08	0.60	89.63	0.96	94.42

Table 2. Benchmark points and dominant decay modes. The "q" notation refers to a sum over the light quarks, d, u, s and c, "l" refers to all leptons, and "ν" to all neutrinos.

JHEP01(2022)120

7 Concluding remarks

It is possible to incorporate a DM candidate within the S_3-symmetric scalar model. The DM candidate requires one of the Higgs doublets to be inert. As S_3 symmetry is assumed and a DM candidate is sought, this requirement imposes constraints on the structure of the Yukawa Lagrangian. As a matter of fact, we found no possible combinations of the exact S_3-symmetric scalar potential and a non-trivial Yukawa Lagrangian, which could accommodate a DM candidate. Hence we require fermions to transform trivially under S_3. When soft-symmetry breaking terms are present, it is possible to construct the Yukawa Lagrangian with a non-trivial S_3 structure. Due to such behaviour an *ad-hoc* S_3 is not appealing in the context of being simultaneously applied to the scalar sector and generating a non-trivial Yukawa sector, while trying to explain DM.

In this work we focused on a specific S_3-symmetric scalar model R-II-1a. As was shown in the paper, this model is compatible with several constraints, both theoretical and experimental. In the IDM and the literature on 3HDMs there is a viable DM high-mass region present. This is not true in our case. The main difference is that the inert-active scalar couplings in the R-II-1a are constrained by the underlying S_3 symmetry and hence the portal couplings are harder to adjust.

We analysed the R-II-1a model numerically. Within the model there are two possible DM candidates present, η and χ. After performing the analysis we found no solutions satisfying all of the constraints with η being the lightest. However, for the χ case there is a range compatible with all constraints, $m_\chi \in [52.5, 89]$ GeV. Constraints in this mass range are compatible with data at the 3-σ level. As compared with the IDM, the R-II-1a model allows solutions in the intermediate-mass range up to somewhat higher values, but can not satisfy all constraints in the high-mass region.

The model differs from the IDM in having two non-inert doublets. The corresponding scalars must be rather light, as shown in figure 12. If these were to be produced at the LHC, they could decay to a pair of scalars from the inert doublet, as well as to final states familiar from the 2HDM. Furthermore, one could imagine direct production of two scalars of the inert doublet, for example via WW or WZ fusion, at rates controlled by the gauge couplings. For all of these cases, the charged $h^\pm$ and neutral η would decay via gauge boson emission to the DM, $h^\pm \to W^\pm\chi$ and $\eta \to Z\chi$, leading to mono-vector events [126, 127].

The present model looks very promising. There are some similarities between this model and the 2HDM. The present framework preserves CP both at the Lagrangian level and by the vacuum. The presence of both $g\,(\eta h^\pm H^\mp)$ and $g\,(\chi h^\pm H^\mp)$ couplings suggests there might be mixing at the one-loop level, but the two diagrams associated with the different charge assignments cancel. Since there is no CP violation in the scalar sector, the Yukawa couplings must be complex and CP is only violated via the CKM matrix. The fermions only couple to one of the active scalars, the one that is a singlet under S_3 since the fermions also transform trivially under S_3. In the S_3-symmetric 3HDM there are also regions of parameter space leading to vacua that violate CP spontaneously, as discussed in refs. [6, 86], showing that the S_3-symmetric 3HDM has a very rich structure.

JHEP01(2022)120

Acknowledgments

It is a pleasure to thank Igor Ivanov, Mikolaj Misiak and Alexander Pukhov for very useful discussions. We thank the referee for pointing out a mistake in the earlier version. PO is supported in part by the Research Council of Norway. The work of AK and MNR was partially supported by Fundação para a Ciência e a Tecnologia (FCT, Portugal) through the projects CFTP-FCT Unit UIDB/00777/2020 and UIDP/00777/2020, CERN/FIS-PAR/0008/2019 and PTDC/FIS-PAR/29436/2017 which are partially funded through POCTI (FEDER), COMPETE, QREN and EU. Furthermore, the work of AK has been supported by the FCT PhD fellowship with reference UI/BD/150735/2020. WK would like to thank the Associateship Scheme at the Abdus Salam International Centre for Theoretical Physics (ICTP) for their support. MNR and PO benefited from discussions that took place at the University of Warsaw during visits supported by the HARMONIA project of the National Science Centre, Poland, under contract UMO-2015/18/M/ST2/00518 (2016-2019), both also thank the University of Bergen and CFTP/ IST/University of Lisbon, where collaboration visits took place.

A Scalar-scalar couplings

For simplicity, the scalar-scalar couplings are presented with the symmetry factor, but without the overall coefficient "$-i$". We denote the "correct" couplings as $g_{\dots} = -ig\,(\dots)$. We shall abbreviate $\mathrm{c}_\theta \equiv \cos\theta$, and $\mathrm{s}_\theta \equiv \sin\theta$, and $\mathrm{t}_\theta \equiv \tan\theta$ for any argument θ.

The trilinear scalar-scalar couplings involving the same species are:

$$g\,(hhh) = 3v\Big[\mathrm{c}_\alpha^3\left(2\left(\lambda_1+\lambda_3\right)\mathrm{s}_\beta - \lambda_4\mathrm{c}_\beta\right) + \left(\lambda_a\mathrm{c}_\beta - 3\lambda_4\mathrm{s}_\beta\right)\mathrm{c}_\alpha^2\mathrm{s}_\alpha + \lambda_a\mathrm{c}_\alpha\mathrm{s}_\alpha^2\mathrm{s}_\beta + 2\lambda_8\mathrm{s}_\alpha^3\mathrm{c}_\beta\Big], \tag{A.1a}$$

$$g\,(HHH) = -3v\Big[\mathrm{s}_\alpha^3\left(2\left(\lambda_1+\lambda_3\right)\mathrm{s}_\beta - \lambda_4\mathrm{c}_\beta\right) + \left(3\lambda_4\mathrm{s}_\beta - \lambda_a\mathrm{c}_\beta\right)\mathrm{c}_\alpha\mathrm{s}_\alpha^2 + \lambda_a\mathrm{c}_\alpha^2\mathrm{s}_\alpha\mathrm{s}_\beta - 2\lambda_8\mathrm{c}_\alpha^3\mathrm{c}_\beta\Big]. \tag{A.1b}$$

The trilinear couplings involving the neutral fields are:

$$g\,(\eta\eta h) = v\left[\mathrm{s}_\alpha\left(3\lambda_4\mathrm{s}_\beta + \lambda_a\mathrm{c}_\beta\right) + \mathrm{c}_\alpha\left(2\left(\lambda_1+\lambda_3\right)\mathrm{s}_\beta + 3\lambda_4\mathrm{c}_\beta\right)\right], \tag{A.2a}$$

$$g\,(\eta\eta H) = v\left[\mathrm{c}_\alpha\left(3\lambda_4\mathrm{s}_\beta + \lambda_a\mathrm{c}_\beta\right) - \mathrm{s}_\alpha\left(2\left(\lambda_1+\lambda_3\right)\mathrm{s}_\beta + 3\lambda_4\mathrm{c}_\beta\right)\right], \tag{A.2b}$$

$$g\,(\chi\chi h) = v\left[\mathrm{s}_\alpha\left(\lambda_4\mathrm{s}_\beta + \lambda_b\mathrm{c}_\beta\right) + \mathrm{c}_\alpha\left(2\left(\lambda_1 - 2\lambda_2 - \lambda_3\right)\mathrm{s}_\beta + \lambda_4\mathrm{c}_\beta\right)\right], \tag{A.2c}$$

$$g\,(\chi\chi H) = v\left[\mathrm{c}_\alpha\left(\lambda_4\mathrm{s}_\beta + \lambda_b\mathrm{c}_\beta\right) - \mathrm{s}_\alpha\left(2\left(\lambda_1 - 2\lambda_2 - \lambda_3\right)\mathrm{s}_\beta + \lambda_4\mathrm{c}_\beta\right)\right], \tag{A.2d}$$

$$g\,(\eta\chi A) = -v\left[\lambda_4\mathrm{c}_{2\beta} + \left(\lambda_2 + \lambda_3 - \lambda_7\right)\mathrm{s}_{2\beta}\right], \tag{A.2e}$$

$$g\,(hhH) = -v\Big[\mathrm{c}_\alpha^3\left(3\lambda_4\mathrm{s}_\beta - \lambda_a\mathrm{c}_\beta\right) + \mathrm{c}_\alpha^2\mathrm{s}_\alpha\left(2\left(3\lambda_1 + 3\lambda_3 - \lambda_a\right)\mathrm{s}_\beta - 3\lambda_4\mathrm{c}_\beta\right) + \lambda_a\mathrm{s}_\alpha^3\mathrm{s}_\beta - 2\mathrm{c}_\alpha\mathrm{s}_\alpha^2\left(3\lambda_4\mathrm{s}_\beta + \left(3\lambda_8 - \lambda_a\right)\mathrm{c}_\beta\right)\Big], \tag{A.2f}$$

JHEP01(2022)120

$$g(hHH) = v\Big[-\mathrm{s}_\alpha^3(3\lambda_4\mathrm{s}_\beta - \lambda_a\mathrm{c}_\beta) + \mathrm{c}_\alpha\mathrm{s}_\alpha^2(2(3\lambda_1+3\lambda_3-\lambda_a)\mathrm{s}_\beta - 3\lambda_4\mathrm{c}_\beta) + \lambda_a\mathrm{c}_\alpha^3\mathrm{s}_\beta + 2\mathrm{c}_\alpha^2\mathrm{s}_\alpha(3\lambda_4\mathrm{s}_\beta + (3\lambda_8-\lambda_a)\mathrm{c}_\beta)\Big], \tag{A.2g}$$

$$g(AAh) = v\Big[\left(\lambda_4\left(2\mathrm{c}_\beta\mathrm{s}_\beta^2 - \mathrm{c}_\beta^3\right) + \lambda_b\mathrm{s}_\beta^3 + 2(\lambda_1+\lambda_3-2\lambda_7)\mathrm{c}_\beta^2\mathrm{s}_\beta\right)\mathrm{c}_\alpha + \left(-\frac{1}{2}\lambda_4\mathrm{s}_{2\beta} - 2(2\lambda_7-\lambda_8)\mathrm{s}_\beta^2 + \lambda_b\mathrm{c}_\beta^2\right)\mathrm{s}_\alpha\mathrm{c}_\beta\Big], \tag{A.2h}$$

$$g(AAH) = v\Big[-\left(\lambda_4\left(2\mathrm{c}_\beta\mathrm{s}_\beta^2 - \mathrm{c}_\beta^3\right) + \lambda_b\mathrm{s}_\beta^3 + 2(\lambda_1+\lambda_3-2\lambda_7)\mathrm{c}_\beta^2\mathrm{s}_\beta\right)\mathrm{s}_\alpha + \left(-\frac{1}{2}\lambda_4\mathrm{s}_{2\beta} - 2(2\lambda_7-\lambda_8)\mathrm{s}_\beta^2 + \lambda_b\mathrm{c}_\beta^2\right)\mathrm{c}_\alpha\mathrm{c}_\beta\Big]. \tag{A.2i}$$

The trilinear couplings involving the charged fields are:

$$g(\eta h^\pm H^\mp) = -\frac{1}{4}v\left[4\lambda_4\mathrm{c}_{2\beta} + (4\lambda_3-\lambda_6-2\lambda_7)\mathrm{s}_{2\beta}\right], \tag{A.3a}$$

$$g(\chi h^\pm H^\mp) = \mp\frac{1}{4}iv(4\lambda_2+\lambda_6-2\lambda_7)\mathrm{s}_{2\beta}, \tag{A.3b}$$

$$g(hH^\pm H^\mp) = -v\Big[\left(\lambda_4\left(\mathrm{c}_\beta^3 - 2\mathrm{c}_\beta\mathrm{s}_\beta^2\right) - \lambda_5\mathrm{s}_\beta^3 - (2\lambda_1+2\lambda_3-\lambda_6-2\lambda_7)\mathrm{c}_\beta^2\mathrm{s}_\beta\right)\mathrm{c}_\alpha + \left(\lambda_4\mathrm{c}_\beta^2\mathrm{s}_\beta - \lambda_5\mathrm{c}_\beta^3 + \lambda_7\mathrm{s}_\beta\mathrm{s}_{2\beta} + (\lambda_6-2\lambda_8)\mathrm{c}_\beta\mathrm{s}_\beta^2\right)\mathrm{s}_\alpha\Big], \tag{A.3c}$$

$$g(HH^\pm H^\mp) = v\Big[\left(\lambda_4\left(\mathrm{c}_\beta^3 - 2\mathrm{c}_\beta\mathrm{s}_\beta^2\right) - \lambda_5\mathrm{s}_\beta^3 - (2\lambda_1+2\lambda_3-\lambda_6-2\lambda_7)\mathrm{c}_\beta^2\mathrm{s}_\beta\right)\mathrm{s}_\alpha - \left(\lambda_4\mathrm{c}_\beta\mathrm{s}_\beta - \lambda_5\mathrm{c}_\beta^2 + (\lambda_6+2\lambda_7-2\lambda_8)\mathrm{s}_\beta^2\right)\mathrm{c}_\alpha\mathrm{c}_\beta\Big], \tag{A.3d}$$

$$g(hh^\pm h^\mp) = v\left[\mathrm{c}_\alpha(2(\lambda_1-\lambda_3)\mathrm{s}_\beta + \lambda_4\mathrm{c}_\beta) + \mathrm{s}_\alpha(\lambda_4\mathrm{s}_\beta + \lambda_5\mathrm{c}_\beta)\right], \tag{A.3e}$$

$$g(Hh^\pm h^\mp) = v\left[-\mathrm{s}_\alpha(2(\lambda_1-\lambda_3)\mathrm{s}_\beta + \lambda_4\mathrm{c}_\beta) + \mathrm{c}_\alpha(\lambda_4\mathrm{s}_\beta + \lambda_5\mathrm{c}_\beta)\right]. \tag{A.3f}$$

The quartic couplings involving the same species are:

$$g(\eta\eta\eta\eta) = g(\chi\chi\chi\chi) = 6(\lambda_1+\lambda_3), \tag{A.4a}$$

$$g(hhhh) = 6\left[(\lambda_1+\lambda_3)\mathrm{c}_\alpha^4 - 2\lambda_4\mathrm{c}_\alpha^3\mathrm{s}_\alpha + \lambda_8\mathrm{s}_\alpha^4 + \frac{1}{4}\lambda_a\mathrm{s}_{2\alpha}^2\right], \tag{A.4b}$$

$$g(HHHH) = 6\left[(\lambda_1+\lambda_3)\mathrm{s}_\alpha^4 + 2\lambda_4\mathrm{c}_\alpha\mathrm{s}_\alpha^3 + \lambda_8\mathrm{c}_\alpha^4 + \frac{1}{4}\lambda_a\mathrm{s}_{2\alpha}^2\right], \tag{A.4c}$$

$$g(AAAA) = 6\left[(\lambda_1+\lambda_3)\mathrm{c}_\beta^4 + 2\lambda_4\mathrm{c}_\beta^3\mathrm{s}_\beta + \lambda_8\mathrm{s}_\beta^4 + \frac{1}{4}\lambda_a\mathrm{s}_{2\beta}^2\right]. \tag{A.4d}$$

JHEP01(2022)120

The quartic couplings involving only the neutral fields are:

$$g(\eta\eta\chi\chi) = 2(\lambda_1+\lambda_3), \tag{A.5a}$$
$$g(\eta\eta AA) = 2(\lambda_1-2\lambda_2-\lambda_3)\,c_\beta^2 - \lambda_4 s_{2\beta} + \lambda_b s_\beta^2, \tag{A.5b}$$
$$g(\chi\chi AA) = 2(\lambda_1+\lambda_3)\,c_\beta^2 - 3\lambda_4 s_{2\beta} + \lambda_a s_\beta^2, \tag{A.5c}$$
$$g(\eta\eta hh) = 2(\lambda_1+\lambda_3)\,c_\alpha^2 + 3\lambda_4 s_{2\alpha} + \lambda_a s_\alpha^2, \tag{A.5d}$$
$$g(\eta\eta hH) = -\frac{1}{2}(2\lambda_1+2\lambda_3-\lambda_a)\,s_{2\alpha} + 3\lambda_4 c_{2\alpha}, \tag{A.5e}$$
$$g(\eta\eta HH) = 2(\lambda_1+\lambda_3)\,s_\alpha^2 - 3\lambda_4 s_{2\alpha} + \lambda_a c_\alpha^2, \tag{A.5f}$$
$$g(\chi\chi hh) = 2(\lambda_1-2\lambda_2-\lambda_3)\,c_\alpha^2 + \lambda_4 s_{2\alpha} + \lambda_b s_\alpha^2, \tag{A.5g}$$
$$g(\chi\chi hH) = \lambda_4 c_{2\alpha} - \frac{1}{2}(2\lambda_1-4\lambda_2-2\lambda_3-\lambda_b)\,s_{2\alpha}, \tag{A.5h}$$
$$g(\chi\chi HH) = 2(\lambda_1-2\lambda_2-\lambda_3)\,s_\alpha^2 - \lambda_4 s_{2\alpha} + \lambda_b c_\alpha^2, \tag{A.5i}$$
$$g(\eta\chi hA) = -c_\alpha\left[2(\lambda_2+\lambda_3)\,c_\beta - \lambda_4 s_\beta\right] - (\lambda_4 c_\beta - 2\lambda_7 s_\beta)\,s_\alpha, \tag{A.5j}$$
$$g(\eta\chi HA) = s_\alpha\left[2(\lambda_2+\lambda_3)\,c_\beta - \lambda_4 s_\beta\right] - (\lambda_4 c_\beta - 2\lambda_7 s_\beta)\,c_\alpha, \tag{A.5k}$$
$$g(hhhH) = -3c_\alpha\left[\lambda_4 c_{3\alpha} + (\lambda_1+\lambda_3-\lambda_8+(\lambda_1+\lambda_3-\lambda_a+\lambda_8)\,c_{2\alpha})\,s_\alpha\right], \tag{A.5l}$$
$$g(hhHH) = \frac{1}{4}\left[3\lambda_1+3\lambda_3+6\lambda_4 s_{4\alpha}+\lambda_a+3\lambda_8-3(\lambda_1+\lambda_3-\lambda_a+\lambda_8)\,c_{4\alpha}\right], \tag{A.5m}$$
$$g(hHHH) = -\frac{3}{2}s_\alpha\left[2\lambda_4 s_{3\alpha} + (\lambda_1+\lambda_3+\lambda_a-3\lambda_8)\,c_\alpha - (\lambda_1+\lambda_3-\lambda_a+\lambda_8)\,c_{3\alpha}\right], \tag{A.5n}$$
$$\begin{aligned} g(AAhh) = {} & -s_{2\alpha}c_\beta\,(\lambda_4 c_\beta + 4\lambda_7 s_\beta) + s_\alpha^2\left(\lambda_b c_\beta^2 + 2\lambda_8 s_\beta^2\right) \\ & + c_\alpha^2\left(2(\lambda_1+\lambda_3)\,c_\beta^2 + \lambda_4 s_{2\beta} + \lambda_b s_\beta^2\right), \end{aligned} \tag{A.5o}$$
$$\begin{aligned} g(AAhH) = {} & -\frac{1}{2}s_{2\alpha}\left[\lambda_1+\lambda_3+\lambda_4 s_{2\beta}-\lambda_8+(\lambda_1+\lambda_3-\lambda_b+\lambda_8)\,c_{2\beta}\right] \\ & - c_{2\alpha}c_\beta\,(\lambda_4 c_\beta + 4\lambda_7 s_\beta), \end{aligned} \tag{A.5p}$$
$$\begin{aligned} g(AAHH) = {} & s_{2\alpha}c_\beta\,(\lambda_4 c_\beta + 4\lambda_7 s_\beta) + c_\alpha^2\left(\lambda_b c_\beta^2 + 2\lambda_8 s_\beta^2\right) \\ & + s_\alpha^2\left(2(\lambda_1+\lambda_3)\,c_\beta^2 + \lambda_4 s_{2\beta} + \lambda_b s_\beta^2\right), \end{aligned} \tag{A.5q}$$

The quartic couplings involving both neutral and charged fields are:

$$g(\eta\eta h^\pm h^\mp) = g(\chi\chi h^\pm h^\mp) = 2(\lambda_1+\lambda_3), \tag{A.6a}$$
$$g(\eta\eta H^\pm H^\mp) = g(\chi\chi H^\mp H^\pm) = 2(\lambda_1-\lambda_3)\,c_\beta^2 - \lambda_4 s_{2\beta} + \lambda_5 s_\beta^2, \tag{A.6b}$$
$$g(\eta h h^\pm H^\mp) = -(2\lambda_3 c_\beta - \lambda_4 s_\beta)\,c_\alpha - \lambda_4 s_\alpha c_\beta + \frac{1}{2}(\lambda_6+2\lambda_7)\,s_\alpha s_\beta, \tag{A.6c}$$
$$g(\eta H h^\pm H^\mp) = (2\lambda_3 c_\beta - \lambda_4 s_\beta)\,s_\alpha - \lambda_4 c_\alpha c_\beta + \frac{1}{2}(\lambda_6+2\lambda_7)\,c_\alpha s_\beta, \tag{A.6d}$$
$$g(\chi h h^\pm H^\mp) = \mp i\left[2\lambda_2 c_\alpha c_\beta + \frac{1}{2}(\lambda_6-2\lambda_7)\,s_\alpha s_\beta\right], \tag{A.6e}$$
$$g(\chi H h^\pm H^\mp) = \mp i\left[-2\lambda_2 s_\alpha c_\beta + \frac{1}{2}(\lambda_6-2\lambda_7)\,c_\alpha s_\beta\right], \tag{A.6f}$$
$$g(hhh^\pm h^\mp) = 2(\lambda_1-\lambda_3)\,c_\alpha^2 + \lambda_4 s_{2\alpha} + \lambda_5 s_\alpha^2, \tag{A.6g}$$

JHEP01(2022)120

$$g\left(hHh^{\pm}h^{\mp}\right) = -\frac{1}{2}\left(2\lambda_1 - 2\lambda_3 - \lambda_5\right)\mathrm{s}_{2\alpha} + \lambda_4\mathrm{c}_{2\alpha}, \tag{A.6h}$$

$$g\left(HHh^{\pm}h^{\mp}\right) = 2\left(\lambda_1 - \lambda_3\right)\mathrm{s}_{\alpha}^2 - \lambda_4\mathrm{s}_{2\alpha} + \lambda_5\mathrm{c}_{\alpha}^2, \tag{A.6i}$$

$$g\left(AAh^{\pm}h^{\mp}\right) = 2\left(\lambda_1 - \lambda_3\right)\mathrm{c}_{\beta}^2 - \lambda_4\mathrm{s}_{2\beta} + \lambda_5\mathrm{s}_{\beta}^2, \tag{A.6j}$$

$$g\left(\eta Ah^{\pm}H^{\mp}\right) = \pm i\left[-2\lambda_2\mathrm{c}_{\beta}^2 + \frac{1}{2}\left(\lambda_6 - 2\lambda_7\right)\mathrm{s}_{\beta}^2\right], \tag{A.6k}$$

$$g\left(\chi Ah^{\pm}H^{\mp}\right) = 2\lambda_3\mathrm{c}_{\beta}^2 - \lambda_4\mathrm{s}_{2\beta} + \frac{1}{2}\left(\lambda_6 + 2\lambda_7\right)\mathrm{s}_{\beta}^2, \tag{A.6l}$$

$$\begin{aligned} g\left(hhH^{\pm}H^{\mp}\right) = {} & \mathrm{c}_{\alpha}^2\left[2\left(\lambda_1 + \lambda_3\right)\mathrm{c}_{\beta}^2 + \lambda_4\mathrm{s}_{2\beta} + \lambda_5\mathrm{s}_{\beta}^2\right] - \lambda_4\mathrm{s}_{2\alpha}\mathrm{c}_{\beta}^2 \\ & + \lambda_5\mathrm{s}_{\alpha}^2\mathrm{c}_{\beta}^2 - \frac{1}{2}\left(\lambda_6 + 2\lambda_7\right)\mathrm{s}_{2\alpha}\mathrm{s}_{2\beta} + 2\lambda_8\mathrm{s}_{\alpha}^2\mathrm{s}_{\beta}^2, \end{aligned} \tag{A.6m}$$

$$\begin{aligned} g\left(hHH^{\pm}H^{\mp}\right) = {} & -\frac{1}{2}\left[\lambda_1 + \lambda_3 + \lambda_4\mathrm{s}_{2\beta} - \lambda_8 + \left(\lambda_1 + \lambda_3 - \lambda_5 + \lambda_8\right)\mathrm{c}_{2\beta}\right]\mathrm{s}_{2\alpha} \\ & - \mathrm{c}_{2\alpha}\mathrm{c}_{\beta}\left[\lambda_4\mathrm{c}_{\beta} + \left(\lambda_6 + 2\lambda_7\right)\mathrm{s}_{\beta}\right], \end{aligned} \tag{A.6n}$$

$$\begin{aligned} g\left(HHH^{\pm}H^{\mp}\right) = {} & \mathrm{s}_{\alpha}^2\left[2\left(\lambda_1 + \lambda_3\right)\mathrm{c}_{\beta}^2 + \lambda_4\mathrm{s}_{2\beta} + \lambda_5\mathrm{s}_{\beta}^2\right] + \lambda_4\mathrm{s}_{2\alpha}\mathrm{c}_{\beta}^2 \\ & + \lambda_5\mathrm{c}_{\alpha}^2\mathrm{c}_{\beta}^2 + \frac{1}{2}\left(\lambda_6 + 2\lambda_7\right)\mathrm{s}_{2\alpha}\mathrm{s}_{2\beta} + 2\lambda_8\mathrm{c}_{\alpha}^2\mathrm{s}_{\beta}^2, \end{aligned} \tag{A.6o}$$

$$g\left(AAH^{\pm}H^{\mp}\right) = 2\left[\left(\lambda_1 + \lambda_3\right)\mathrm{c}_{\beta}^4 + 2\lambda_4\mathrm{c}_{\beta}^3\mathrm{s}_{\beta} + \frac{1}{4}\lambda_a\mathrm{s}_{2\beta}^2 + \lambda_8\mathrm{s}_{\beta}^4\right]. \tag{A.6p}$$

The quartic couplings involving only the charged fields are:

$$g\left(h^{\pm}h^{\pm}h^{\mp}h^{\mp}\right) = 4\left(\lambda_1 + \lambda_3\right), \tag{A.7a}$$

$$g\left(H^{\pm}H^{\pm}H^{\mp}H^{\mp}\right) = 4\left[\left(\lambda_1 + \lambda_3\right)\mathrm{c}_{\beta}^4 + 2\lambda_4\mathrm{c}_{\beta}^3\mathrm{s}_{\beta} + \frac{1}{4}\lambda_a\mathrm{s}_{2\beta}^2 + \lambda_8\mathrm{s}_{\beta}^4\right], \tag{A.7b}$$

$$g\left(h^{\pm}h^{\pm}H^{\mp}H^{\mp}\right) = 4\left[\left(\lambda_2 + \lambda_3\right)\mathrm{c}_{\beta}^2 - \frac{1}{2}\lambda_4\mathrm{s}_{2\beta} + \lambda_7\mathrm{s}_{\beta}^2\right], \tag{A.7c}$$

$$g\left(h^{\pm}h^{\mp}H^{\pm}H^{\mp}\right) = 2\left(\lambda_1 - \lambda_2\right)\mathrm{c}_{\beta}^2 - 2\lambda_4\mathrm{s}_{2\beta} + \left(\lambda_5 + \lambda_6\right)\mathrm{s}_{\beta}^2. \tag{A.7d}$$

B Theory constraints

We impose certain data-independent theory constraints on the models.

B.1 Stability

Necessary, but not sufficient, conditions for the stability of an S_3-symmetric 3HDM were provided in ref. [89]. In ref. [6], based on the approach of refs. [78, 128], necessary and sufficient conditions for models with $\lambda_4 = 0$ were discussed. It was later pointed out in ref. [129] that parameterisation used in ref. [78], and hence in ref. [6], is not correct,[3] and

[3]Namely, the complex product between two different unit spinors relied on six degrees of freedom. However, one of those can be expressed in terms of the other quantities, see section III-C of ref. [129]. The following positivity condition for models with $\lambda_4 = 0$ (B.28) [6]

$$\lambda_5 + \min\left(0, \lambda_6 - 2\left|\lambda_7\right|\right) > -2\sqrt{\left(\lambda_1 + \min\left(0, -\lambda_2, \lambda_3\right)\right)\lambda_8}, \tag{B.1}$$

yields an over-constrained λ parameter space.

JHEP01(2022)120

one would arrive at a value of the potential which would be lower than what actually is possible to achieve within the space available.

In our case, due to the freedom of the λ_4 coupling, which breaks the O(2) symmetry, the stability conditions are rather involved. We parameterise the SU(2) doublets as

$$h_i = ||h_i||\hat{h}_i, \quad i = \{1, 2, S\}, \tag{B.2}$$

where the norms of the spinors $||h_i||$ are parameterised in terms of the spherical coordinates

$$||h_1|| = r\cos\gamma\sin\theta, \qquad ||h_2|| = r\sin\gamma\sin\theta, \qquad ||h_S|| = r\cos\theta, \tag{B.3}$$

and $\hat{h}_i$ are unit spinors

$$\hat{h}_1 = \begin{pmatrix} 0 \\ 1 \end{pmatrix}, \qquad \hat{h}_2 = \begin{pmatrix} \sin\alpha_2 \\ \cos\alpha_2\, e^{i\beta_2} \end{pmatrix}, \qquad \hat{h}_S = e^{i\delta}\begin{pmatrix} \sin\alpha_3 \\ \cos\alpha_3\, e^{i\beta_3} \end{pmatrix}, \tag{B.4}$$

where $r \geq 0$, $\gamma \in [0, \pi/2]$, $\theta \in [0, \pi/2]$, and $\alpha_i \in [0, \pi/2]$, $\beta_i \in [0, 2\pi]$, $\delta \in [0, 2\pi]$. The positivity condition is satisfied, with only the quartic part being relevant, for

$$V_4 = \sum_i \lambda_i A_i \geq 0, \quad \forall\,\{\gamma, \theta, \alpha_i, \beta_i, \delta\}, \tag{B.5}$$

where

$$A_1 = \sin^4\theta, \tag{B.6a}$$

$$A_2 = -\sin^2(2\gamma)\sin^4\theta\cos^2\alpha_2\sin^2\beta_2, \tag{B.6b}$$

$$A_3 = \left(\cos^4\gamma + \sin^4\gamma\right)\sin^4\theta - \frac{1}{2}\sin^2(2\gamma)\sin^4\theta\left[\sin^2\alpha_2 - \cos^2\alpha_2\cos(2\beta_2)\right], \tag{B.6c}$$

$$\begin{aligned} A_4 = \sin(2\theta)\sin^2\theta\sin\gamma\Big(&\cos(2\gamma)\sin\alpha_2\sin\alpha_3\cos\delta \\ &- \cos\alpha_2\cos\alpha_3\Big[\sin^2\gamma\cos(\beta_2 - \beta_3 - \delta) \\ &- \cos^2\gamma\left\{2\cos\left(\beta_2 - \beta_3 - \delta\right) + \cos\left(\beta_2 + \beta_3 + \delta\right)\right\}\Big]\Big), \end{aligned} \tag{B.6d}$$

$$A_5 = \frac{1}{4}\sin^2(2\theta), \tag{B.6e}$$

$$\begin{aligned} A_6 = \frac{1}{4}\sin^2(2\theta)\Big(&\cos^2\gamma\cos^2\alpha_3 + \sin^2\gamma\Big[\cos^2\alpha_2\cos^2\alpha_3 \\ &+ \sin\alpha_3\left\{\sin(2\alpha_2)\cos\alpha_3\cos\left(\beta_2 - \beta_3\right) + \sin^2\alpha_2\sin\alpha_3\right\}\Big]\Big), \end{aligned} \tag{B.6f}$$

$$\begin{aligned} A_7 = \frac{1}{2}\sin^2(2\theta)\Big(&\cos^2\gamma\cos^2\alpha_3\cos\left(2\beta_3 + 2\delta\right) \\ &+ \sin^2\gamma\Big[\cos^2\alpha_2\cos^2\alpha_3\cos\left(2\beta_2 - 2\beta_3 - 2\delta\right) \\ &+ \sin\alpha_3\left\{\sin^2\alpha_2\sin\alpha_3\cos(2\delta) + \sin(2\alpha_2)\cos\alpha_3\cos\left(\beta_2 - \beta_3 - 2\delta\right)\right\}\Big]\Big), \end{aligned} \tag{B.6g}$$

$$A_8 = \cos^4\theta. \tag{B.6h}$$

JHEP01(2022)120

Conditions	$V_4 > 0$	Conditions from ref. [89]
$\gamma = \frac{\pi}{4}$, $\theta = \alpha_2 = \frac{\pi}{2}$	λ_1	(4a)
$\theta = 0$	λ_8	(4b)
$\gamma = \frac{\pi}{4}$, $\theta = \frac{\pi}{2}$, $\alpha_2 = 0$, $\beta_2 = \{0, \frac{\pi}{2}\}$	$\lambda_1 + \lambda_3$ $\lambda_1 - \lambda_2$	(4c) and (4d)
$\gamma = 0$, $\delta = 0$, $\tan\theta = \sqrt{\frac{\lambda_8}{\sqrt{(\lambda_1+\lambda_3)\lambda_8}}}$, $\alpha_3 = \{0, \frac{\pi}{2}\}$, $\beta_3 = \{0, \frac{\pi}{2}\}$	$\lambda_5 + \min(0, \lambda_6 - 2\lvert\lambda_7\rvert)$ $+2\sqrt{(\lambda_1+\lambda_3)\lambda_8}$	(4e) and (4f)
$\theta = \frac{\pi}{4}$, $\gamma = \frac{\pi}{2}$, $\alpha_2 = \alpha_3 = \frac{\pi}{2}$, $\delta = \{\pi, 2\pi\}$	$\lambda_1 + \lambda_3 \pm 2\lambda_4 + \lambda_5$ $+\lambda_6 + 2\lambda_7 + \lambda_8$	(4g)

Table 3. Reproduction of the necessary stability conditions of ref. [89] in terms of the parameterisation given by (B.2).

First, we check if the necessary stability constraints are satisfied, see table 3. Next, with the help of the Mathematica function NMinimize, using different algorithms, a further numerical minimisation of the potential is performed.

B.2 Unitarity

The tree-level unitarity conditions for the S_3-symemtric 3HDM were presented in ref. [89]. The unitarity limit is evaluated enforcing the absolute values of the eigenvalues Λ_i of the scattering matrix to be within a specific limit. In our scan we assume that one is given by the value $|\Lambda_i| \leq 16\pi$ [130]. Some authors prefer a more severe bound $|\Lambda_i| \leq 8\pi$ [131, 132]. We compare the impact of both in figures 2.

B.3 Perturbativity

The perturbativity check is split into two parts: couplings are assumed to be within the limit $|\lambda_i| \leq 4\pi$, the overall strength of the quartic scalar-scalar interactions is limited by $|g_{\varphi_i\varphi_j\varphi_k\varphi_l}| \leq 4\pi$.

For the R-II-1a model, the list of the quartic scalar interactions $g_{\varphi_i\varphi_j\varphi_k\varphi_l}$ can be found in appendix A. From the interactions $\eta\eta\eta\eta$ and $\chi\chi\chi\chi$ (A.4a), it follows that $0 < \lambda_1 + \lambda_3 \leq 2\pi/3$. Evaluation of other couplings is more involved.

JHEP01(2022)120

C Supplementary equations

C.1 Di-photon decays

The one-loop spin-dependent functions are

$$\mathcal{F}_1 = 2 + 3\tau + 3\tau(2-\tau)f(\tau), \tag{C.1a}$$

$$\mathcal{F}_{1/2}^i = \begin{cases} -2\tau[1+(1-\tau)f(\tau)], & i = S, \\ -2\tau f(\tau), & i = P, \end{cases} \tag{C.1b}$$

$$\mathcal{F}_0 = \tau[1-\tau f(\tau)], \tag{C.1c}$$

where

$$\tau_i = \frac{4m_i^2}{m_h^2}, \tag{C.2}$$

and

$$f(\tau) = \begin{cases} \arcsin^2\left(\frac{1}{\sqrt{\tau}}\right), & \tau \geq 1, \\ -\frac{1}{4}\left[\ln\left(\frac{1+\sqrt{1-\tau}}{1-\sqrt{1-\tau}}\right) - i\pi\right]^2, & \tau < 1. \end{cases} \tag{C.3}$$

C.2 V and U matrices

From refs. [133, 134] we determine the V and U matrices[4] for R-II-1a in the Higgs basis (4.33)

$$\begin{pmatrix} \sin(\alpha+\beta)\,h + \cos(\alpha+\beta)\,H + iG^0 \\ -\cos(\alpha+\beta)\,h + \sin(\alpha+\beta)\,H + iA \\ \eta + i\chi \end{pmatrix} = V \begin{pmatrix} G^0 \\ A \\ h \\ H \\ \eta \\ \chi \end{pmatrix}, \tag{C.4a}$$

with

$$V = \begin{pmatrix} i & 0 & \sin(\alpha+\beta) & \cos(\alpha+\beta) & 0 & 0 \\ 0 & i & -\cos(\alpha+\beta) & \sin(\alpha+\beta) & 0 & 0 \\ 0 & 0 & 0 & 0 & 1 & i \end{pmatrix}, \tag{C.4b}$$

and

$$\begin{pmatrix} G^+ \\ H^+ \\ h^+ \end{pmatrix} = U \begin{pmatrix} G^+ \\ H^+ \\ h^+ \end{pmatrix}, \text{ with } U = \mathcal{I}_3. \tag{C.4c}$$

[4]Note that "U" here should not be confused with the electroweak precision observable "U".

JHEP01(2022)120

References

[1] Planck collaboration, *Planck* 2018 *results. VI. Cosmological parameters*, *Astron. Astrophys.* **641** (2020) A6 [*Erratum ibid.* **652** (2021) C4] [arXiv:1807.06209] [INSPIRE].

[2] J.F. Gunion, H.E. Haber, G.L. Kane and S. Dawson, *The Higgs hunter's guide*, *Front. Phys.* **80** (2000) 1 [INSPIRE].

[3] G.C. Branco, P.M. Ferreira, L. Lavoura, M.N. Rebelo, M. Sher and J.P. Silva, *Theory and phenomenology of two-Higgs-doublet models*, *Phys. Rept.* **516** (2012) 1 [arXiv:1106.0034] [INSPIRE].

[4] N.G. Deshpande and E. Ma, *Pattern of symmetry breaking with two Higgs doublets*, *Phys. Rev. D* **18** (1978) 2574 [INSPIRE].

[5] R. Barbieri, L.J. Hall and V.S. Rychkov, *Improved naturalness with a heavy Higgs: an alternative road to LHC physics*, *Phys. Rev. D* **74** (2006) 015007 [hep-ph/0603188] [INSPIRE].

[6] D. Emmanuel-Costa, O.M. Ogreid, P. Osland and M.N. Rebelo, *Spontaneous symmetry breaking in the S_3-symmetric scalar sector*, *JHEP* **02** (2016) 154 [*Erratum ibid.* **08** (2016) 169] [arXiv:1601.04654] [INSPIRE].

[7] O.M. Ogreid, P. Osland and M.N. Rebelo, *A simple method to detect spontaneous CP-violation in multi-Higgs models*, *JHEP* **08** (2017) 005 [arXiv:1701.04768] [INSPIRE].

[8] ATLAS collaboration, *Observation of a new particle in the search for the Standard Model Higgs boson with the ATLAS detector at the LHC*, *Phys. Lett. B* **716** (2012) 1 [arXiv:1207.7214] [INSPIRE].

[9] CMS collaboration, *Observation of a new boson at a mass of* 125 *GeV with the CMS experiment at the LHC*, *Phys. Lett. B* **716** (2012) 30 [arXiv:1207.7235] [INSPIRE].

[10] G. Bélanger, F. Boudjema, A. Pukhov and A. Semenov, *Dark matter direct detection rate in a generic model with MicrOMEGAs* 2.2, *Comput. Phys. Commun.* **180** (2009) 747 [arXiv:0803.2360] [INSPIRE].

[11] G. Bélanger, F. Boudjema, A. Pukhov and A. Semenov, *MicrOMEGAs*3*: a program for calculating dark matter observables*, *Comput. Phys. Commun.* **185** (2014) 960 [arXiv:1305.0237] [INSPIRE].

[12] D. Barducci et al., *Collider limits on new physics within MicrOMEGAs*4.3, *Comput. Phys. Commun.* **222** (2018) 327 [arXiv:1606.03834] [INSPIRE].

[13] V. Silveira and A. Zee, *Scalar phantoms*, *Phys. Lett. B* **161** (1985) 136 [INSPIRE].

[14] J. McDonald, *Gauge singlet scalars as cold dark matter*, *Phys. Rev. D* **50** (1994) 3637 [hep-ph/0702143] [INSPIRE].

[15] C.P. Burgess, M. Pospelov and T. ter Veldhuis, *The minimal model of nonbaryonic dark matter: a singlet scalar*, *Nucl. Phys. B* **619** (2001) 709 [hep-ph/0011335] [INSPIRE].

[16] B. Patt and F. Wilczek, *Higgs-field portal into hidden sectors*, hep-ph/0605188 [INSPIRE].

[17] V. Barger, P. Langacker, M. McCaskey, M.J. Ramsey-Musolf and G. Shaughnessy, *LHC phenomenology of an extended Standard Model with a real scalar singlet*, *Phys. Rev. D* **77** (2008) 035005 [arXiv:0706.4311] [INSPIRE].

JHEP01(2022)120

[18] S. Andreas, T. Hambye and M.H.G. Tytgat, *WIMP dark matter, Higgs exchange and DAMA*, *JCAP* **10** (2008) 034 [arXiv:0808.0255] [INSPIRE].

[19] Y. Mambrini, *Higgs searches and singlet scalar dark matter: combined constraints from XENON*100 *and the LHC*, *Phys. Rev. D* **84** (2011) 115017 [arXiv:1108.0671] [INSPIRE].

[20] I. Low, P. Schwaller, G. Shaughnessy and C.E.M. Wagner, *The dark side of the Higgs boson*, *Phys. Rev. D* **85** (2012) 015009 [arXiv:1110.4405] [INSPIRE].

[21] A. Djouadi, O. Lebedev, Y. Mambrini and J. Quevillon, *Implications of LHC searches for Higgs-portal dark matter*, *Phys. Lett. B* **709** (2012) 65 [arXiv:1112.3299] [INSPIRE].

[22] X.-G. He, B. Ren and J. Tandean, *Hints of Standard Model Higgs boson at the LHC and light dark matter searches*, *Phys. Rev. D* **85** (2012) 093019 [arXiv:1112.6364] [INSPIRE].

[23] J.M. Cline, K. Kainulainen, P. Scott and C. Weniger, *Update on scalar singlet dark matter*, *Phys. Rev. D* **88** (2013) 055025 [*Erratum ibid.* **92** (2015) 039906] [arXiv:1306.4710] [INSPIRE].

[24] L. Feng, S. Profumo and L. Ubaldi, *Closing in on singlet scalar dark matter: LUX, invisible Higgs decays and gamma-ray lines*, *JHEP* **03** (2015) 045 [arXiv:1412.1105] [INSPIRE].

[25] A. Beniwal et al., *Combined analysis of effective Higgs portal dark matter models*, *Phys. Rev. D* **93** (2016) 115016 [arXiv:1512.06458] [INSPIRE].

[26] A. Cuoco, B. Eiteneuer, J. Heisig and M. Krämer, *A global fit of the γ-ray galactic center excess within the scalar singlet Higgs portal model*, *JCAP* **06** (2016) 050 [arXiv:1603.08228] [INSPIRE].

[27] X.-G. He and J. Tandean, *New LUX and PandaX-II results illuminating the simplest Higgs-portal dark matter models*, *JHEP* **12** (2016) 074 [arXiv:1609.03551] [INSPIRE].

[28] J.A. Casas, D.G. Cerdeño, J.M. Moreno and J. Quilis, *Reopening the Higgs portal for single scalar dark matter*, *JHEP* **05** (2017) 036 [arXiv:1701.08134] [INSPIRE].

[29] GAMBIT collaboration, *Status of the scalar singlet dark matter model*, *Eur. Phys. J. C* **77** (2017) 568 [arXiv:1705.07931] [INSPIRE].

[30] G. Bélanger, K. Kannike, A. Pukhov and M. Raidal, *Z_3 scalar singlet dark matter*, *JCAP* **01** (2013) 022 [arXiv:1211.1014] [INSPIRE].

[31] P. Ko and Y. Tang, *Self-interacting scalar dark matter with local Z_3 symmetry*, *JCAP* **05** (2014) 047 [arXiv:1402.6449] [INSPIRE].

[32] M. Cirelli, N. Fornengo and A. Strumia, *Minimal dark matter*, *Nucl. Phys. B* **753** (2006) 178 [hep-ph/0512090] [INSPIRE].

[33] M. Cirelli, A. Strumia and M. Tamburini, *Cosmology and astrophysics of minimal dark matter*, *Nucl. Phys. B* **787** (2007) 152 [arXiv:0706.4071] [INSPIRE].

[34] M. Cirelli, R. Franceschini and A. Strumia, *Minimal dark matter predictions for galactic positrons, anti-protons, photons*, *Nucl. Phys. B* **800** (2008) 204 [arXiv:0802.3378] [INSPIRE].

[35] M. Cirelli and A. Strumia, *Minimal dark matter: model and results*, *New J. Phys.* **11** (2009) 105005 [arXiv:0903.3381] [INSPIRE].

[36] T. Hambye, F.S. Ling, L. Lopez Honorez and J. Rocher, *Scalar multiplet dark matter*, *JHEP* **07** (2009) 090 [*Erratum ibid.* **05** (2010) 066] [arXiv:0903.4010] [INSPIRE].

JHEP01(2022)120

[37] Y. Cai, W. Chao and S. Yang, *Scalar septuplet dark matter and enhanced $h \to \gamma\gamma$ decay rate*, *JHEP* **12** (2012) 043 [arXiv:1208.3949] [INSPIRE].

[38] K. Earl, K. Hartling, H.E. Logan and T. Pilkington, *Constraining models with a large scalar multiplet*, *Phys. Rev. D* **88** (2013) 015002 [arXiv:1303.1244] [INSPIRE].

[39] C. Garcia-Cely, A. Ibarra, A.S. Lamperstorfer and M.H.G. Tytgat, *Gamma-rays from heavy minimal dark matter*, *JCAP* **10** (2015) 058 [arXiv:1507.05536] [INSPIRE].

[40] E. Del Nobile, M. Nardecchia and P. Panci, *Millicharge or decay: a critical take on minimal dark matter*, *JCAP* **04** (2016) 048 [arXiv:1512.05353] [INSPIRE].

[41] E. Ma, *Verifiable radiative seesaw mechanism of neutrino mass and dark matter*, *Phys. Rev. D* **73** (2006) 077301 [hep-ph/0601225] [INSPIRE].

[42] J. Kubo, E. Ma and D. Suematsu, *Cold dark matter, radiative neutrino mass, $\mu \to e\gamma$, and neutrinoless double beta decay*, *Phys. Lett. B* **642** (2006) 18 [hep-ph/0604114] [INSPIRE].

[43] S. Andreas, M.H.G. Tytgat and Q. Swillens, *Neutrinos from inert doublet dark matter*, *JCAP* **04** (2009) 004 [arXiv:0901.1750] [INSPIRE].

[44] D. Majumdar and A. Ghosal, *Dark matter candidate in a heavy Higgs model — direct detection rates*, *Mod. Phys. Lett. A* **23** (2008) 2011 [hep-ph/0607067] [INSPIRE].

[45] L. Lopez Honorez, E. Nezri, J.F. Oliver and M.H.G. Tytgat, *The inert doublet model: an archetype for dark matter*, *JCAP* **02** (2007) 028 [hep-ph/0612275] [INSPIRE].

[46] M. Gustafsson, E. Lundstrom, L. Bergstrom and J. Edsjo, *Significant gamma lines from inert Higgs dark matter*, *Phys. Rev. Lett.* **99** (2007) 041301 [astro-ph/0703512] [INSPIRE].

[47] T. Hambye and M.H.G. Tytgat, *Electroweak symmetry breaking induced by dark matter*, *Phys. Lett. B* **659** (2008) 651 [arXiv:0707.0633] [INSPIRE].

[48] Q.-H. Cao, E. Ma and G. Rajasekaran, *Observing the dark scalar doublet and its impact on the Standard-Model Higgs boson at colliders*, *Phys. Rev. D* **76** (2007) 095011 [arXiv:0708.2939] [INSPIRE].

[49] E. Lundstrom, M. Gustafsson and J. Edsjo, *The inert doublet model and LEP II limits*, *Phys. Rev. D* **79** (2009) 035013 [arXiv:0810.3924] [INSPIRE].

[50] P. Agrawal, E.M. Dolle and C.A. Krenke, *Signals of inert doublet dark matter in neutrino telescopes*, *Phys. Rev. D* **79** (2009) 015015 [arXiv:0811.1798] [INSPIRE].

[51] E. Nezri, M.H.G. Tytgat and G. Vertongen, *e^+ and $\bar{p}$ from inert doublet model dark matter*, *JCAP* **04** (2009) 014 [arXiv:0901.2556] [INSPIRE].

[52] E.M. Dolle and S. Su, *The inert dark matter*, *Phys. Rev. D* **80** (2009) 055012 [arXiv:0906.1609] [INSPIRE].

[53] C. Arina, F.-S. Ling and M.H.G. Tytgat, *IDM and iDM or the inert doublet model and inelastic dark matter*, *JCAP* **10** (2009) 018 [arXiv:0907.0430] [INSPIRE].

[54] E. Dolle, X. Miao, S. Su and B. Thomas, *Dilepton signals in the inert doublet model*, *Phys. Rev. D* **81** (2010) 035003 [arXiv:0909.3094] [INSPIRE].

[55] L. Lopez Honorez and C.E. Yaguna, *The inert doublet model of dark matter revisited*, *JHEP* **09** (2010) 046 [arXiv:1003.3125] [INSPIRE].

[56] X. Miao, S. Su and B. Thomas, *Trilepton signals in the inert doublet model*, *Phys. Rev. D* **82** (2010) 035009 [arXiv:1005.0090] [INSPIRE].

JHEP01(2022)120

[57] L. Lopez Honorez and C.E. Yaguna, *A new viable region of the inert doublet model*, *JCAP* **01** (2011) 002 [arXiv:1011.1411] [INSPIRE].

[58] D. Sokolowska, *Dark matter data and constraints on quartic couplings in IDM*, arXiv:1107.1991 [INSPIRE].

[59] B. Swiezewska and M. Krawczyk, *Diphoton rate in the inert doublet model with a* 125 *GeV Higgs boson*, *Phys. Rev. D* **88** (2013) 035019 [arXiv:1212.4100] [INSPIRE].

[60] A. Goudelis, B. Herrmann and O. Stål, *Dark matter in the inert doublet model after the discovery of a Higgs-like boson at the LHC*, *JHEP* **09** (2013) 106 [arXiv:1303.3010] [INSPIRE].

[61] M. Krawczyk, D. Sokolowska, P. Swaczyna and B. Swiezewska, *Constraining inert dark matter by $R_{\gamma\gamma}$ and WMAP data*, *JHEP* **09** (2013) 055 [arXiv:1305.6266] [INSPIRE].

[62] A. Arhrib, Y.-L.S. Tsai, Q. Yuan and T.-C. Yuan, *An updated analysis of inert Higgs doublet model in light of the recent results from LUX, PLANCK, AMS-*02 *and LHC*, *JCAP* **06** (2014) 030 [arXiv:1310.0358] [INSPIRE].

[63] A. Ilnicka, M. Krawczyk and T. Robens, *Inert doublet model in light of LHC run I and astrophysical data*, *Phys. Rev. D* **93** (2016) 055026 [arXiv:1508.01671] [INSPIRE].

[64] M.A. Díaz, B. Koch and S. Urrutia-Quiroga, *Constraints to dark matter from inert Higgs doublet model*, *Adv. High Energy Phys.* **2016** (2016) 8278375 [arXiv:1511.04429] [INSPIRE].

[65] A. Belyaev, G. Cacciapaglia, I.P. Ivanov, F. Rojas-Abatte and M. Thomas, *Anatomy of the inert two Higgs doublet model in the light of the LHC and non-LHC dark matter searches*, *Phys. Rev. D* **97** (2018) 035011 [arXiv:1612.00511] [INSPIRE].

[66] J. Kalinowski, W. Kotlarski, T. Robens, D. Sokolowska and A.F. Zarnecki, *Benchmarking the inert doublet model for e^+e^- colliders*, *JHEP* **12** (2018) 081 [arXiv:1809.07712] [INSPIRE].

[67] M. Aoki, S. Kanemura and H. Yokoya, *Reconstruction of inert doublet scalars at the International Linear Collider*, *Phys. Lett. B* **725** (2013) 302 [arXiv:1303.6191] [INSPIRE].

[68] M. Hashemi, M. Krawczyk, S. Najjari and A.F. Żarnecki, *Production of inert scalars at the high energy e^+e^- colliders*, *JHEP* **02** (2016) 187 [arXiv:1512.01175] [INSPIRE].

[69] J. Kalinowski, W. Kotlarski, T. Robens, D. Sokolowska and A.F. Zarnecki, *Exploring inert scalars at CLIC*, *JHEP* **07** (2019) 053 [arXiv:1811.06952] [INSPIRE].

[70] M. Merchand and M. Sher, *Constraints on the parameter space in an inert doublet model with two active doublets*, *JHEP* **03** (2020) 108 [arXiv:1911.06477] [INSPIRE].

[71] V. Keus, S.F. King, S. Moretti and D. Sokolowska, *Dark matter with two inert doublets plus one Higgs doublet*, *JHEP* **11** (2014) 016 [arXiv:1407.7859] [INSPIRE].

[72] V. Keus, S.F. King, S. Moretti and D. Sokolowska, *Observable heavy Higgs dark matter*, *JHEP* **11** (2015) 003 [arXiv:1507.08433] [INSPIRE].

[73] A. Cordero et al., *Dark matter signals at the LHC from a* 3*HDM*, *JHEP* **05** (2018) 030 [arXiv:1712.09598] [INSPIRE].

[74] A. Cordero-Cid et al., *CP violating scalar dark matter*, *JHEP* **12** (2016) 014 [arXiv:1608.01673] [INSPIRE].

JHEP01(2022)120

[75] LUX collaboration, *Results from a search for dark matter in the complete LUX exposure*, *Phys. Rev. Lett.* **118** (2017) 021303 [arXiv:1608.07648] [INSPIRE].

[76] PANDAX-II collaboration, *Dark matter results from 54-ton-day exposure of PandaX-II experiment*, *Phys. Rev. Lett.* **119** (2017) 181302 [arXiv:1708.06917] [INSPIRE].

[77] XENON collaboration, *Dark matter search results from a one ton-year exposure of XENON1T*, *Phys. Rev. Lett.* **121** (2018) 111302 [arXiv:1805.12562] [INSPIRE].

[78] B. Grzadkowski, O.M. Ogreid and P. Osland, *Natural multi-Higgs model with dark matter and CP-violation*, *Phys. Rev. D* **80** (2009) 055013 [arXiv:0904.2173] [INSPIRE].

[79] B. Grzadkowski, O.M. Ogreid, P. Osland, A. Pukhov and M. Purmohammadi, *Exploring the CP-violating inert-doublet model*, *JHEP* **06** (2011) 003 [arXiv:1012.4680] [INSPIRE].

[80] P. Osland, A. Pukhov, G.M. Pruna and M. Purmohammadi, *Phenomenology of charged scalars in the CP-violating inert-doublet model*, *JHEP* **04** (2013) 040 [arXiv:1302.3713] [INSPIRE].

[81] A.C.B. Machado and V. Pleitez, *A model with two inert scalar doublets*, *Annals Phys.* **364** (2016) 53 [arXiv:1205.0995] [INSPIRE].

[82] V. Keus, S.F. King and S. Moretti, *Three-Higgs-doublet models: symmetries, potentials and Higgs boson masses*, *JHEP* **01** (2014) 052 [arXiv:1310.8253] [INSPIRE].

[83] E.C.F.S. Fortes, A.C.B. Machado, J. Montaño and V. Pleitez, *Scalar dark matter candidates in a two inert Higgs doublet model*, *J. Phys. G* **42** (2015) 105003 [arXiv:1407.4749] [INSPIRE].

[84] A. Aranda, J. Hernández-Sánchez, R. Noriega-Papaqui and C.A. Vaquera-Araujo, *Yukawa textures or dark doublets from two Higgs doublet models with Z_3 symmetry*, arXiv:1410.1194 [INSPIRE].

[85] A. Aranda et al., *Z_3 symmetric inert $(2+1)$-Higgs-doublet model*, *Phys. Rev. D* **103** (2021) 015023 [arXiv:1907.12470] [INSPIRE].

[86] A. Kunčinas, O.M. Ogreid, P. Osland and M.N. Rebelo, *S_3-inspired three-Higgs-doublet models: a class with a complex vacuum*, *Phys. Rev. D* **101** (2020) 075052 [arXiv:2001.01994] [INSPIRE].

[87] J. Kubo, H. Okada and F. Sakamaki, *Higgs potential in minimal S_3 invariant extension of the standard model*, *Phys. Rev. D* **70** (2004) 036007 [hep-ph/0402089] [INSPIRE].

[88] T. Teshima, *Higgs potential in S_3 invariant model for quark/lepton mass and mixing*, *Phys. Rev. D* **85** (2012) 105013 [arXiv:1202.4528] [INSPIRE].

[89] D. Das and U.K. Dey, *Analysis of an extended scalar sector with S_3 symmetry*, *Phys. Rev. D* **89** (2014) 095025 [*Erratum ibid.* **91** (2015) 039905] [arXiv:1404.2491] [INSPIRE].

[90] E. Derman and H.-S. Tsao, *$\mathrm{SU}(2) \times \mathrm{U}(1) \times S_n$ flavor dynamics and a bound on the number of flavors*, *Phys. Rev. D* **20** (1979) 1207 [INSPIRE].

[91] A. Kuncinas, *Properties of S_3-symmetric three-Higgs-doublet models*, master thesis, University of Bergen, Bergen, Norway (2019).

[92] ALEPH, DELPHI, L3, OPAL and LEP ELECTROWEAK collaborations, *Electroweak measurements in electron-positron collisions at W-boson-pair energies at LEP*, *Phys. Rept.* **532** (2013) 119 [arXiv:1302.3415] [INSPIRE].

JHEP01(2022)120

[93] A. Pierce and J. Thaler, *Natural dark matter from an unnatural Higgs boson and new colored particles at the TeV scale*, *JHEP* **08** (2007) 026 [hep-ph/0703056] [INSPIRE].

[94] A. Arbey, F. Mahmoudi, O. Stål and T. Stefaniak, *Status of the charged Higgs boson in two Higgs doublet models*, *Eur. Phys. J. C* **78** (2018) 182 [arXiv:1706.07414] [INSPIRE].

[95] Particle Data Group collaboration, *Review of particle physics*, *PTEP* **2020** (2020) 083C01 [INSPIRE].

[96] B. Grinstein and M.B. Wise, *Weak radiative B meson decay as a probe of the Higgs sector*, *Phys. Lett. B* **201** (1988) 274 [INSPIRE].

[97] W.-S. Hou and R.S. Willey, *Effects of extended Higgs sector on loop induced B decays*, *Nucl. Phys. B* **326** (1989) 54 [INSPIRE].

[98] B. Grinstein, R.P. Springer and M.B. Wise, *Strong interaction effects in weak radiative $\bar{B}$ meson decay*, *Nucl. Phys. B* **339** (1990) 269 [INSPIRE].

[99] A.J. Buras, M. Misiak, M. Münz and S. Pokorski, *Theoretical uncertainties and phenomenological aspects of $B \to X_s\gamma$ decay*, *Nucl. Phys. B* **424** (1994) 374 [hep-ph/9311345] [INSPIRE].

[100] P. Ciafaloni, A. Romanino and A. Strumia, *Two loop QCD corrections to charged Higgs mediated $b \to s\gamma$ decay*, *Nucl. Phys. B* **524** (1998) 361 [hep-ph/9710312] [INSPIRE].

[101] M. Ciuchini, G. Degrassi, P. Gambino and G.F. Giudice, *Next-to-leading QCD corrections to $B \to X_s\gamma$: Standard Model and two Higgs doublet model*, *Nucl. Phys. B* **527** (1998) 21 [hep-ph/9710335] [INSPIRE].

[102] F. Borzumati and C. Greub, *2HDMs predictions for $\bar{B} \to X_s\gamma$ in NLO QCD*, *Phys. Rev. D* **58** (1998) 074004 [hep-ph/9802391] [INSPIRE].

[103] C. Bobeth, M. Misiak and J. Urban, *Matching conditions for $b \to s\gamma$ and $b \to s$ gluon in extensions of the Standard Model*, *Nucl. Phys. B* **567** (2000) 153 [hep-ph/9904413] [INSPIRE].

[104] C. Bobeth, M. Misiak and J. Urban, *Photonic penguins at two loops and m_t dependence of $BR[B \to X_s\ell^+\ell^-]$*, *Nucl. Phys. B* **574** (2000) 291 [hep-ph/9910220] [INSPIRE].

[105] P. Gambino and M. Misiak, *Quark mass effects in $\bar{B} \to X_s\gamma$*, *Nucl. Phys. B* **611** (2001) 338 [hep-ph/0104034] [INSPIRE].

[106] K. Cheung and O.C.W. Kong, *Can the two Higgs doublet model survive the constraint from the muon anomalous magnetic moment as suggested?*, *Phys. Rev. D* **68** (2003) 053003 [hep-ph/0302111] [INSPIRE].

[107] M. Misiak and M. Steinhauser, *Three loop matching of the dipole operators for $b \to s\gamma$ and $b \to sg$*, *Nucl. Phys. B* **683** (2004) 277 [hep-ph/0401041] [INSPIRE].

[108] M. Czakon, U. Haisch and M. Misiak, *Four-loop anomalous dimensions for radiative flavour-changing decays*, *JHEP* **03** (2007) 008 [hep-ph/0612329] [INSPIRE].

[109] T. Hermann, M. Misiak and M. Steinhauser, *$\bar{B} \to X_s\gamma$ in the two Higgs doublet model up to next-to-next-to-leading order in QCD*, *JHEP* **11** (2012) 036 [arXiv:1208.2788] [INSPIRE].

[110] M. Misiak et al., *Updated NNLO QCD predictions for the weak radiative B-meson decays*, *Phys. Rev. Lett.* **114** (2015) 221801 [arXiv:1503.01789] [INSPIRE].

JHEP01(2022)120

[111] M. Misiak and M. Steinhauser, *Weak radiative decays of the B meson and bounds on $M_{H^\pm}$ in the two-Higgs-doublet model*, *Eur. Phys. J. C* **77** (2017) 201 [arXiv:1702.04571] [INSPIRE].

[112] M. Misiak, A. Rehman and M. Steinhauser, *Towards $\bar{B} \to X_s\gamma$ at the NNLO in QCD without interpolation in m_c*, *JHEP* **06** (2020) 175 [arXiv:2002.01548] [INSPIRE].

[113] M. Misiak and M. Steinhauser, *NNLO QCD corrections to the $\bar{B} \to X_s\gamma$ matrix elements using interpolation in m_c*, *Nucl. Phys. B* **764** (2007) 62 [hep-ph/0609241] [INSPIRE].

[114] J.R. Ellis, M.K. Gaillard and D.V. Nanopoulos, *A phenomenological profile of the Higgs boson*, *Nucl. Phys. B* **106** (1976) 292 [INSPIRE].

[115] M.A. Shifman, A.I. Vainshtein, M.B. Voloshin and V.I. Zakharov, *Low-energy theorems for Higgs boson couplings to photons*, *Sov. J. Nucl. Phys.* **30** (1979) 711 [*Yad. Fiz.* **30** (1979) 1368] [INSPIRE].

[116] F. Wilczek, *Decays of heavy vector mesons into Higgs particles*, *Phys. Rev. Lett.* **39** (1977) 1304 [INSPIRE].

[117] H.M. Georgi, S.L. Glashow, M.E. Machacek and D.V. Nanopoulos, *Higgs bosons from two gluon annihilation in proton proton collisions*, *Phys. Rev. Lett.* **40** (1978) 692 [INSPIRE].

[118] J.R. Ellis, M.K. Gaillard, D.V. Nanopoulos and C.T. Sachrajda, *Is the mass of the Higgs boson about* 10 *GeV?*, *Phys. Lett. B* **83** (1979) 339 [INSPIRE].

[119] T.G. Rizzo, *Gluon final states in Higgs boson decay*, *Phys. Rev. D* **22** (1980) 178 [*Addendum ibid.* **22** (1980) 1824] [INSPIRE].

[120] ATLAS collaboration, *Combination of searches for invisible Higgs boson decays with the ATLAS experiment*, *Phys. Rev. Lett.* **122** (2019) 231801 [arXiv:1904.05105] [INSPIRE].

[121] CMS collaboration, *Search for invisible decays of a Higgs boson produced through vector boson fusion in proton-proton collisions at $\sqrt{s} = 13$ TeV*, *Phys. Lett. B* **793** (2019) 520 [arXiv:1809.05937] [INSPIRE].

[122] F. Boudjema and E. Chopin, *Double Higgs production at the linear colliders and the probing of the Higgs selfcoupling*, *Z. Phys. C* **73** (1996) 85 [hep-ph/9507396] [INSPIRE].

[123] A. Belyaev, N.D. Christensen and A. Pukhov, *CalcHEP* 3.4 *for collider physics within and beyond the Standard Model*, *Comput. Phys. Commun.* **184** (2013) 1729 [arXiv:1207.6082] [INSPIRE].

[124] F. Staub, *From superpotential to model files for FeynArts and CalcHep/CompHEP*, *Comput. Phys. Commun.* **181** (2010) 1077 [arXiv:0909.2863] [INSPIRE].

[125] F. Staub, *SARAH* 4*: a tool for (not only SUSY) model builders*, *Comput. Phys. Commun.* **185** (2014) 1773 [arXiv:1309.7223] [INSPIRE].

[126] ATLAS collaboration, *Search for dark matter in events with a hadronically decaying vector boson and missing transverse momentum in pp collisions at $\sqrt{s} = 13$ TeV with the ATLAS detector*, *JHEP* **10** (2018) 180 [arXiv:1807.11471] [INSPIRE].

[127] CMS collaboration, *Search for new particles in events with energetic jets and large missing transverse momentum in proton-proton collisions at $\sqrt{s} = 13$ TeV*, Tech. Rep. CMS-PAS-EXO-20-004, CERN, Geneva, Switzerland (2021).

[128] A.W. El Kaffas, W. Khater, O.M. Ogreid and P. Osland, *Consistency of the two Higgs doublet model and CP-violation in top production at the LHC*, *Nucl. Phys. B* **775** (2007) 45 [hep-ph/0605142] [INSPIRE].

JHEP01(2022)120

[129] F.S. Faro and I.P. Ivanov, *Boundedness from below in the* U(1) × U(1) *three-Higgs-doublet model*, *Phys. Rev. D* **100** (2019) 035038 [arXiv:1907.01963] [INSPIRE].

[130] B.W. Lee, C. Quigg and H.B. Thacker, *Weak interactions at very high-energies: the role of the Higgs boson mass*, *Phys. Rev. D* **16** (1977) 1519 [INSPIRE].

[131] M. Lüscher and P. Weisz, *Is there a strong interaction sector in the standard lattice Higgs model?*, *Phys. Lett. B* **212** (1988) 472 [INSPIRE].

[132] W.J. Marciano, G. Valencia and S. Willenbrock, *Renormalization group improved unitarity bounds on the Higgs boson and top quark masses*, *Phys. Rev. D* **40** (1989) 1725 [INSPIRE].

[133] W. Grimus, L. Lavoura, O.M. Ogreid and P. Osland, *A precision constraint on multi-Higgs-doublet models*, *J. Phys. G* **35** (2008) 075001 [arXiv:0711.4022] [INSPIRE].

[134] W. Grimus, L. Lavoura, O.M. Ogreid and P. Osland, *The oblique parameters in multi-Higgs-doublet models*, *Nucl. Phys. B* **801** (2008) 81 [arXiv:0802.4353] [INSPIRE].

JHEP01(2022)120